3D volumetric isotopological meshing for finite element and isogeometric based reduced order modeling

T. Maquart, Y. Wenfeng, T. Elguedj, A. Gravouil, M. Rochette

Version of Record: https://www.sciencedirect.com/science/article/pii/S0045782519307017
Manuscript_489a19e076503aa0c45257bab891cb05

3D volumetric isotopological meshing for finite element and isogeometric based reduced order modeling

T. Maquart[a,b], Y. Wenfeng[b], T. Elguedj[a,*], A. Gravouil[a], M. Rochette[b]

[a] *Univ Lyon, INSA-Lyon, CNRS UMR5259, LaMCoS, F-69621, France*
[b] *ANSYS Research & Development, France*

Abstract

This paper presents a generic framework to construct 3D structured volumetric meshes of complicated geometry and arbitrary topology. Structured meshes are well-suited for reduced order model applications with geometric parameters. For that purpose, we use the triangulated solid 3D model's boundary provided from B-Rep CAD (Boundary-Representation in Computer Aided Design) models. The input triangulated mesh is decomposed into a set of cuboids in two steps: pants decomposition and cuboid decomposition. Both segmentations understand the geometry and features of meshes. Cuboid decomposition splits a surface into a set of quadrilateral patches which can define a volumetric layout of the associated boundary surface. Using aligned global parameterization, patches of the cuboid decomposition are re-positioned on the surface in a way to achieve low overall distortion, and alignment to principal curvature directions and sharp features. The optimization process is thought to design cross fields with topological and geometrical constraints. Using the optimized cuboid decomposition, a volumetric layout is extracted. Based on the global parameterization and the structured volumetric layout previously computed, a 3D volumetric parameterization is deducted. For different geometrical instances with the same topology but different geometries, the proposed method allows to have the same representation: 3D volumetric isotopological meshes holding the same connectivity. MEG-IsoHex method is introduced to compare fields on 3D hexahedral meshes. The efficiency and the robustness of the proposed approach are illustrated through a remeshing case for large deformations and reduced order models using isogeometric analysis.

Keywords: Cuboid decomposition; Topology; Global parameterization; 3D B-Spline; Parametric geometry; Reduced order modeling.

1. Introduction

Since few years, numerous applications in computational physics are dedicated to reduced order modeling. Indeed, a real benefit is brought by determining complex solutions in real-time. For example, onboard sophisticated computations in fighter aircrafts become possible. Nowadays problems are multidimensional models involving multidimensional spaces, see, e.g. Chinesta et al. [1, 2]. Domains of applications are changing and new emerging issues in the physics world require reliable fast resolution. For example, Niroomandi et al. [3] have used an offline step to reduce non-linear responses of living tissues. Some researchers include geometrical parameters in order to optimize shape structures [4], but it remains a tedious task to build the required suitable meshes to avoid any projection step. Understanding these difficulties, we need isotopological 3D meshes, i.e., a structured information for all members of the population to be reduced.

*I am corresponding author; Laboratoire de Mécanique des Contacts et des Structures Université de Lyon, CNRS, INSA-Lyon UMR5259 27 bis avenue Jean Capelle - F69621 Villeurbanne Cedex France. Phone number : +33 (0)4 72 43 84 52
Email addresses: tristan.maquart@insa-lyon.fr (T. Maquart), tristan.maquart@hotmail.fr (T. Maquart), wenfeng.ye@ansys.com (Y. Wenfeng), thomas.elguedj@insa-lyon.fr (T. Elguedj), anthony.gravouil@insa-lyon.fr (A. Gravouil), michel.rochette@ansys.com (M. Rochette)
URL: http://lamcos.insa-lyon.fr/ (T. Elguedj)

IsoGeometric Analysis [5, 6] is a recent method that represents the geometry better than standard Finite Element meshes and has better continuity properties between elements. Indeed, this method uses the same type of mathematical representation for both geometry and solution fields. This computational approach offers the possibility to fill the gap between design and analysis. Treating geometry with such new tools is obvious for geometrical parameterizations needs.

Problem statement

In this paper, we seek to build 3D volumetric meshes whose properties are specific to reduced order modeling applications. The aim is to be able to compare different shapes with different geometries but with the same structure, i.e., with the same topology. In other words, we want to analyze field differences between distinctives meshes of a population. These meshes are greatly appreciated in reduced order modeling [4, 7–9]. Figure 1 states the problematic using trivariate B-Spline meshes used in IGA. Since these spline meshes need to be structured, relevant hexahedron extraction is straightforward. The most desirable mesh properties usually are:

- Minimize the number of high valence nodes.
- Alignement with features, curvature directions and boundaries.
- Determine high quality elements, close to a hexahedron as possible.
- Constrain the number of elements and connectivity to obtain *isotopological* meshes.
- Locate mesh nodes and elements on features to get *homologous* comparable meshes.

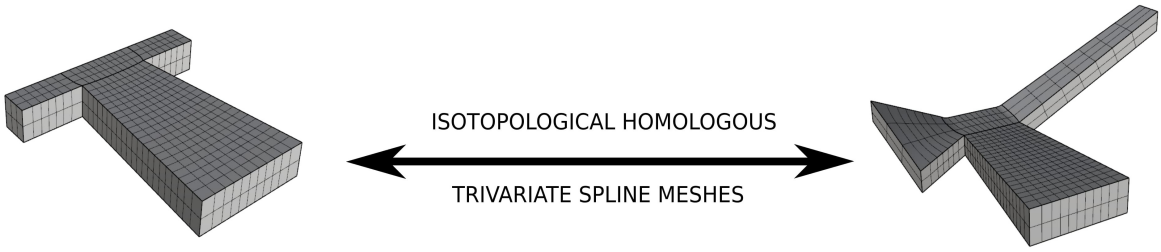

Figure 1: To compare fields on meshes efficiently, the discretization needs to be the same and homologous.

Overview

We give a method to compute quality 3D hexahedral or trivariate B-Spline meshes with specific properties needed in parametric analysis. We strive to build isotopological homologous meshes from triangulated surface provided by B-Rep CAD. Such meshes are generated using objects with complex geometry and arbitrary topology. This work is based on smart geometry-comprehensive algorithms which interact together.

To do this, we present an integrated pipeline partitioning the input from triangulated surface to relevant domains useful to compute comparable 3D hexahedral meshes. Hexahedral meshes are degree-1 B-Spline meshes. Firstly, we seek to understand the geometry while decomposing the mesh. This task is done with geometry-aware pants decomposition and feature-aware-cuboid decomposition algorithms. We treat input surfaces with pants decomposition approaches [10–13]. Thereafter, we perform cuboid decomposition [14–16] splitting each pants patch into a coarse quadrilateral mesh lying on triangulated mesh features as possible. Novelty is brought by locating properly high valence nodes of the quadrilateral layout. Secondly, a

surface optimized global parameterization helps us to define a high quality quadrilateral mesh. Based on the approach introduced by Campen and Kobbelt [17], quadrilateral patches embedded on the studied surface are optimized in a way to minimize the surface parameterization distortion. We design cross fields to guide the parameterization [18–20]. Topological properties of such direction fields are entirely provided from the layout. The third main significant contribution is topology based. We use topology concepts throughout the pipeline to design volumetric layouts from unstructured CAD geometry. From the beginning to the end, decomposed topologies are constrained and analyzed in order to build structured 3D meshes using unstructured ones. We present properties of $2, 3$-dimensional manifolds embedded in $\mathbb{R}^3$ for 2-dimensional manifolds to 3-dimensional manifolds conversion. Close links between quadrilateral layout and volumetric layout are then determined. Suitable volumetric layouts are then an essential scheme to build required trivariate isogeometric and hexahedral meshes.

Reduced order modeling is a tedious task that requires structured large amount of data. All geometric instances of the population must satisfy isotopological and homologous mesh properties to be efficiently compared and studied whether it is their geometries or their embedded data that is targeted. The issue of having isotopological meshes is adressed by generating the same parameterization for all members of the given population. Figure 2 provides a rapid understanding of the proposed approach.

To summarize, improvements can be divided in three main parts. First, the decomposition pipeline is revisited to understand the geometry in section 2.3. Then using aligned global parameterization computed from a geometrically relevant cross field, we extract a surface parameterization in section 2.4 and 2.5. Optimized parameterization and resulting quadrilateral layout are then used to determine a volumetric layout. Topological properties enabling surface to volumetric conversion are formulated in section 2.6. Section 3 presents some examples to illustrate the efficiency of the method.

2. Building isotopological homologous 3D meshes for snapshots computations: MEG-IsoHex method

In this section we present a 3D hexahedral isotopological meshing process method. We seek to compute 3D hexahderal or trivariate spline instances suitable for reduced order modeling applications. Hexahedral mesh topology needs to be the same among all snapshots. We also strive to place nodes and elements in a geometry-aware manner, i.e., all isotopological meshes have homologous points in the whole mesh. Because the workflow is thought from the beginning to build such meshes for reduced order modeling tasks, topological properties are constrained throughout the proposed process.

2.1. Topology and parameterization prerequisites

Topology is the study of properties like continuity, connectedness and boundaries of a space that are preserved under continuous deformations, such as bending and stretching, but not tearing and gluing. A *homeomorphism* is an *isomorphism* that admits a continuous function between two topological equivalent spaces that has a continous inverse function. We are interested in transformations that preserve all the topological properties of a given space. *Homeomorphic* spaces admit a *homeomorphism* between them, thus topological spaces are equivalent. See Hatcher [21] for more details.

A surface M is a **2-manifold**, i.e., a topological space in which each point has a neighborhood *homeomorphic* to either the plane $\mathbb{R}^2$ or the closed half plane $\mathbb{R}^2_+$. Points with closed half-plane neighborhood are defined as the boundary ∂M of the surface M. In the following we investigate only connected, orientable, differentiable and compact surfaces with boundaries. **Genus** of a connected and orientable surface M (i.e., a 2-*manifold* embedded in $\mathbb{R}^3$) is the maximum number of non-intersecting closed curves which can be drawn on it without disconnecting the surface. With these definitions, taking into account a genus-g surface M possibly with b boundary components, we can now define the topological invariant. This invariant used to classify surfaces is called **Euler characteristic**: $\chi(M) = 2 - 2g - b$. We note that surfaces with different *Euler characteristic* cannot be *homeomorphic*. In addition, surfaces with the same *Euler characteristic* are not necessarily *homemorphic* in the general case.

We define a **homology basis** for M to be any set of $2g$ *cycles* whose *homology classes* generate the first *homology group* H_1 [22]. Cutting along these cycles yields a genus-0 surface. The set of all *handle* and

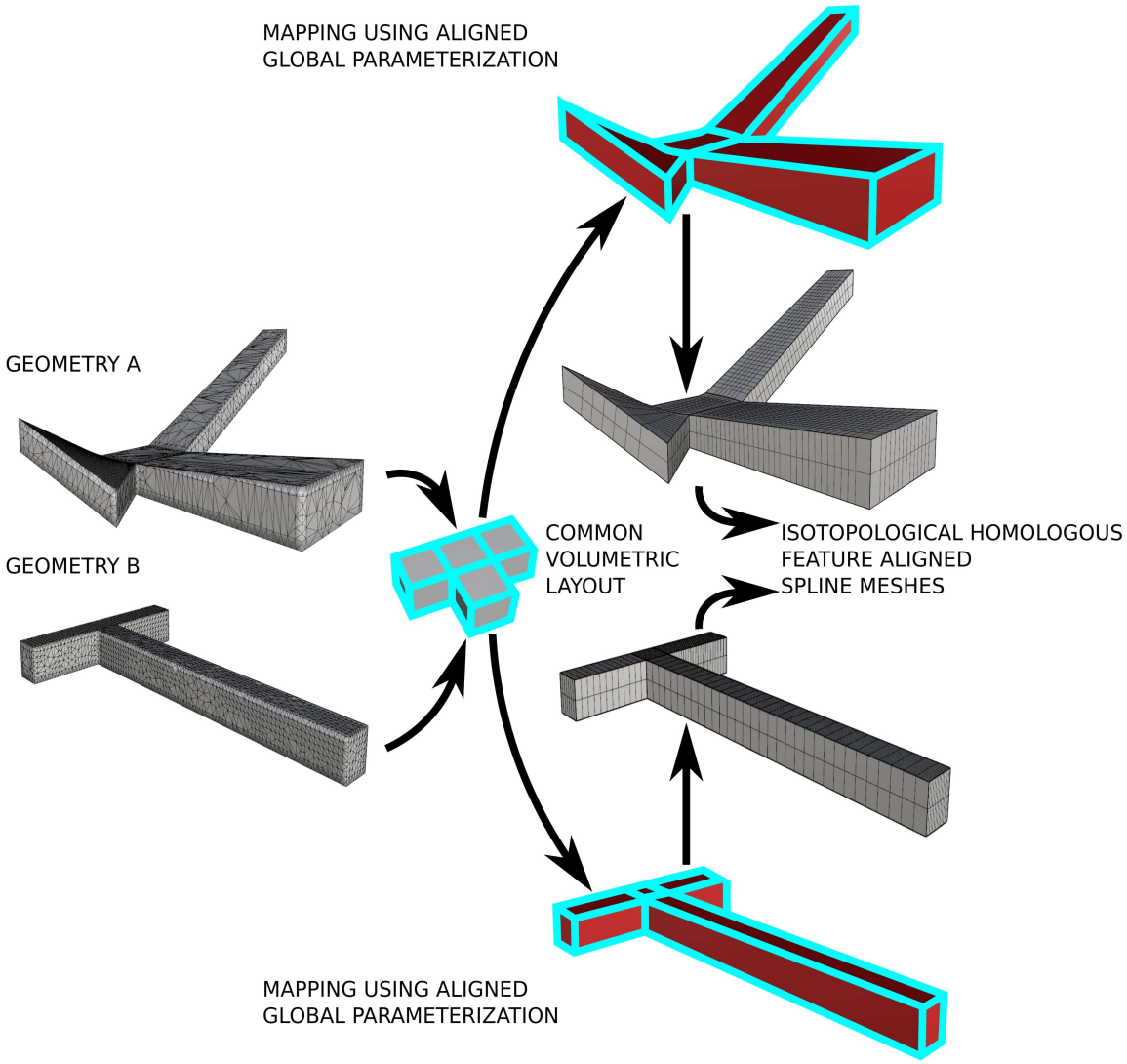

Figure 2: MEG-IsoHex method. Building isotopological homologous feature-aligned hexahedral or spline meshes from triangulated meshes with the same topology. Resulting isotopological meshes have non-uniform isotropy.

tunnel loops form a *homology basis*. Suppose a closed surface $M \subset \mathbb{R}^3$ separates $\mathbb{R}^3$ into a bounded space $\mathbb{I}$ and an unbounded space $\mathbb{O}$. *handle* and *tunnel* loops on M can be defined as follows. A loop a_i is a *tunnel* if it spans a disk in the unbounded space $\mathbb{O}$. A loop b_i is a *handle* if it spans a disk in the bounded space $\mathbb{I}$.

Pants decomposition has been studied by Hatcher et al. [23], work has been done to find the optimal segmentation of a given surface into relevant *pants* patches [13] using the shortest homology basis [24]. Geometry-aware *pants decomposition* has been also investigated by Zhang and Li [10]. Li et al. [12] developed a *pants decomposition* framework to compute maps between surfaces with arbitrary topologies. An example of pants decomposition using a homology basis is shown in figure 3.

Let $M_{g,b}$ be a surface of genus g with b boundary components. A *pants decomposition* of $M_{g,b}$ is a collection of pairwise disjoint simple cycles that splits the surface into *pants* patches. Each *pants* patch is a genus-0 surface (topological sphere) with 3 boundaries. We assume that M is a surface with negative *Euler characteristic*, i.e., M is none of the surfaces $M_{0,0}$ (topological sphere), $M_{0,1}$ (topological disk), $M_{0,2}$

(topological cylinder) and $M_{1,0}$ (topological torus). For a surface $M_{g,b}$, pants decomposition is possible if and only if $\chi(M) = 2 - 2g - b \leq -1$. In this case *pants decompositions* of M do exist, and each *pants decomposition* consists of $3g + b - 3$ curves and divides M into $2g + b - 2$ *pants* patches.

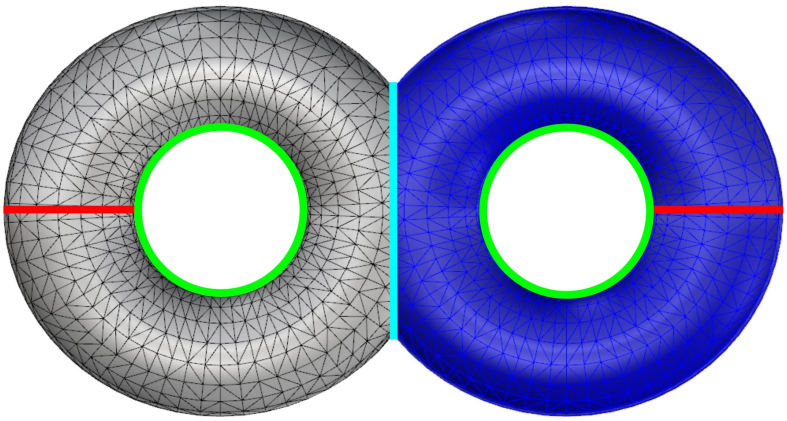

Figure 3: Pants decomposition and topological properties of a double torus. A double torus is a genus-2 surface without boundaries and has Euler characteristic $\chi = 2 - 2g - b = -2$. Pants decomposition provides two pants (gray and blue meshes) by cutting along handle loops and using symmetry (symmetry loop is depicted in cyan). Homology basis is composed by two handle loops and two tunnel loops respectively depicted in red and green.

A **direction field** defined on a surface M is a tangent unit vector field: at each point of the surface, there exists a direction u such that $\|\mathbf{u}\| = 1$ and $\mathbf{u}.\mathbf{n} = 0$, where $\mathbf{n}$ is the normal of M. A *N-symmetry direction field* $\mathcal{U}$ is a multivalued *direction field*: at each point of the surface M, there exists a *N-symmetry direction* $\mathbf{u}$ which is a set of N directions $\{\mathbf{u}_1, \mathbf{u}_2, ..., \mathbf{u}_{N-1}, \mathbf{u}_N\}$ preserved by rotations of $2\pi/N$ around the normal $\mathbf{n}$ of M. Let us introduce the **Poincaré-Hopf theorem** for a connected, compact and differentiable *2-dimensional manifold* M in equation (1). We can define it with $\mathcal{C}$ a *4-symmetry direction field* and n_s isolated singularities of indices $I^i_{\mathcal{C}}$ embedded on the surface M. Field singularities can be isolated in boundaries locations. If M has boundaries, the vector field must be pointing in the outward normal direction along them. There exists a trade beetween the **boundary number theorem** [20, 25] and the **Poincaré-Hopf theorem**. For higher field symmetries than a vector field, the behavior near boundaries must be correctly analyzed.

$$\sum_{i=1}^{n_s} I^i_{\mathcal{C}} = \chi(M). \tag{1}$$

Many different techniques of mapping exist. In our case we are interested in mappings or **parameterizations** which map a surface M embedded in $\mathbb{R}^3$ to a canonical domain D in $\mathbb{R}^2$. The ideal *parameterization* is isometric, i.e., it fully preserves areas and angles. For surfaces, an isometric *parameterization* is not possible in the general case. Therefore, approaches to *2-dimensional manifold* parameterization attempt to find a mapping which is either *conformal* with no angular distortion, or *equiareal* with no area distortion. *Conformal* mappings always exist into one of the three following canonical domains: the sphere, the plane, and the hyperbolic space. The **isometric theorem** guarantees that a conformal equiareal mapping is isometric. In the following we consider a triangulated surface M with vertices V, edges E and faces F, and only disk-like surfaces for parameterization. We use discrete *harmonic* mapping to solve such parameterizations. *Harmonic* mappings have attributes derived from conformal parameterization, but there is no guarantee on angles. To proceed we construct a *harmonic* function $f : M \longrightarrow \mathbb{R}$ such that $\Delta f = 0$. Harmonic maps minimize *Dirichlet* energy:

$$E_D(f) = \frac{1}{2}\int_M \|\nabla f\|^2 dM. \tag{2}$$

The surface boundary ∂M is first mapped to the boundary of the parametric domain and then the parameterization for the interior vertices is obtained by solving the linear system:

$$\Delta_w f(v_i) = \sum_{j \in N_i} w_{ij}(f(v_j) - f(v_i)). \tag{3}$$

Where v_i, $v_j \in V$, N_i is the neigborhood of v_i, and w_{ij} is the scalar weight assigned to the oriented edge $e_{ij}(v_i, v_j)$. Recently Saboret et al. [26] have implemented a CGAL package handling some of the state-of-the-art surface parameterization methods. Different parameterization methods assign different weights w_{ij}. The first definition of weight was introduced by Tutte [27]. In the parameter space, each vertex is placed at the barycenter of its neighbors. To the best of our knowledge, the most used weights are the mean value coordinates weights introduced by Floater [28]. Our need is a mapping where f is harmonic, the parametric space $\subset \mathbb{R}^2$ is convex and the boundary ∂M is mapped homeomorphically in the parametric space. With these conditions and positive vertices weights for discrete maps, f has to be bijective according to the **Rado-Kneser-Choquet theorem**.

2.2. Advanced topology prerequisites

In this section we provide well-known results on the generalized *Euler characteristic*. We introduce here the generalized *Euler characteristic* for the following purposes. First, we define **cohomology groups**. They are invariant information attached to a specific group. The cohomology groups $\mathbf{H}^n$ looks at the groups actions between a group G in an associated $G - module\ M$. Elements of a n-dimensional group G^n representing n-simplices:

$$\mathbf{H}^n = \mathbf{H}(G^n, M). \tag{4}$$

Thus, we can characterize the general formulation of *Euler characteristic* using previous definition of *cohomology groups*. Characteristic is computed regarding the properties of the associated **simplicial complex** in cases of meshes, i.e., their n-dimensional counterparts. *Simplicial complexes* have a certain combinatorial nature and allow numerical computations. We want to define geometrical objects with both continous and combinatorial properties. **CW-Complex** (also known by Closure-finite Weak-topology) entities k_i have been introduced to answer the needs of homotopy theory in *simplicial complexes*. In other words, properties that allow continuous deformations for combinatorial structures are needed. Generalized *Euler characteristic* of a compact n-dimensional manifold M is the alternate sum of the lengths of the *cohomology groups* $\mathbf{H}^i$ (5). This characteristic can be also obtained simply from **Betti numbers** b_i. *Betti numbers* are used to differentiate topological spaces, it can be also used for *simplicial complexes* or *CW-complexes*.

$$\chi(M) = \sum_{i=0}^{n<\infty} (-1)^i |\mathbf{H}^i| = \sum_{i=0}^{n<\infty} (-1)^i k_i(M) = \sum_{i=0}^{n<\infty} (-1)^i b_i(M). \tag{5}$$

In the following, we explain quickly the links between *Euler Characteristic* and **Gauss-Bonnet theorem**. We seek to find valuable information on indices, number and locations of singularities of a given field. The *Gauss-Bonnet theorem* associates the total **Gaussian curvature** and total **geodesic curvature** to a topological invariant. In other words, this theorem states the connection between topology and geometry in an integral form:

$$\int_M K dS + \int_{\partial M = \gamma(s)} kg\ ds = 2\pi\chi(M). \tag{6}$$

Where K is the *Gaussian curvature* on the surface of area S and kg the *geodesic curvature* along boundary cycles $\gamma(s)$. Since this theorem establishes a relation between geometry and a topological invariant, it is better to locate field singularities $I^i_{\mathcal{C}}$ near areas with non-zero *Gaussian curvature*.

2.3. Smart model decomposition

This section is divided in two main parts: pants decomposition and cuboid decomposition. They are the steps of surface segmentation in order to obtain the final cuboid decomposition of a complex triangulated geometry with an arbitrary topology. We give fundamental pants and cuboid decomposition tools so as to understand the following developments.

Pants decomposition

Pants decomposition provides a canonical decomposition scheme for common surfaces. $\chi = -1$ for a pants patch, so pants have a very simple topology. In the following, handle and tunnel loops are computed using the work of Dey et al. [29]. We improve an existing pants decomposition algorithm from Al-Akhras [30] by adding geometry considerations. Given a homology basis formed by handle and tunnel loops, we can take a subset H composed of g simple pairwise disjoint handle loops $\{h_1, h_2, ..., h_{g-1}, h_g\}$. Slicing surface M with b boundary components along its g handle loops will lead to a genus-0 surface with $2g+b$ boundary components denoted as $W = \{w_1, ..., w_{2g+b}\}$. We iteratively pick two boundaries w_i and w_j among all non-repeating and commutative combinations from W and compute a new simple cycle w_{ij} to bound them, i.e., w_{ij} is homotopic to $w_i \circ w_j$. The three cycles w_i, w_j and w_{ij} bound a pants patch T_k. We remove this pants patch T_k from M. The remaining patch is still genus-0 but its boundary number reduces by 1: the two cycles w_i and w_j are removed, and one new cycle w_{ij} is inserted. This is iteratively performed until $|W| = 3$. Different geometric criteria exist to determine w_{ij} for the pants decomposition. Shortest length, areas of minimum Gaussian curvature and symmetry can be used. Geometric criterion has to be adapted to the mesh M. Furthermore, features are very useful to locate w_{ij}. It is the main idea behind geometry-aware pants decomposition using sharp points S. This idea is formulated in algorithm 1. Geometry-aware pants decomposition is one of the first steps of smart model decomposition illustrated in figure 4.

Compared to the method of Al-Akhras [30], we introduce an extension to enumerate the entire space of topological pants decomposition possibilities at each step. In other words, instead of picking 2 boundaries in an arbitrary manner, we suggest to take all couples of 2 boundaries among all non-repeating and commutative combinations when determining a pants patch relative to the considered step. Besides, giving some feature points, our new algorithm is able to determine a pant by slicing the mesh along a cycle passing across these locations. By doing this, user manual inputs are reduced to feature points selection in order to guide the decomposition passing through these points of interest.

Pants decomposition of a given object is not unique and clearly depends on the set of loops choosen to create it, i.e., it depends on the geometric criterion used to obtain these loops as observed by Dey et al. [29] and Zhang and Li [10]. With our proposed geometry-aware pants decomposition algorithm, the result is robust based on the small set of points provided by the user.

Cuboid decomposition

First, we seek to decompose a pants patch into a set of $n_{\mathbb{Q}}$ quadrilateral patches of a quadrilateral layout $\mathbb{Q}$ embedded in the triangulated surface. Optimal number of quadrilateral patches depends on the features we want to replicate in the computed output mesh. Li et al. [16] presented a method that generates the same quadrilateral patches number per pants patch with a given user data input. Al-Akhras et al. [31] has developed a cuboid decomposition technique without sharp features considerations and with a simple cuboid decomposition scheme. The concept is to generate corners and polyedges on each pants patch T_i and decompose it into a set of 4 cuboids, each having 8 corners and 12 polyedges in order to construct a volumetric parameterization. For the following purposes, we give just a general algorithm information where the most relevant specifications are provided. As input, we have 3 boundaries B_1, B_2 and B_3 obtained from a pants patch. We process these pants patches one by one in an arbitrary order. To guarantee cuboid corner alignment, when we determine one pants patch's result, we transfer its corners on the boundaries of the adjacent pants patches if they are not processed yet. We use a new extension to handle more complicated geometry taking into account sharp features and geometry detailed in our very recent work [32]. On each

Algorithm 1 Geometry-aware pants decomposition

Input Triangulated genus-g surface M with b boundary components and its g geometrically relevant handle loops.

$k = 1$.
Slice M along all its handle loops and get a genus-0 surface M_k with $2g + b$ boundaries.
Put all boundaries of M_k in a set $W = \{w_1, ..., w_{2g+b}\}$.
While $|W| > 3$ **do**
  Build (or reset) an empty set of loops $L = \{0\}$.
  Compute N_c: all non-repeating and commutative combinations ($\dim(N_c) = \frac{Size(W)!}{2!(Size(W)-2)!}$).
  For all couples $[w_i, w_j]$ in N_c:
    Compute a cycle w_{ij} homotopic to $w_i \circ w_j$ given by a geometric criterion or a set of points S.
    Add loop to L.
  End For
  Sort relevant loops in $L = \{l_1, ..., l_{\dim(N_c)}\}$ using a geometric criterion to obtain the optimal w_{ij} cycle.
  $\{w_1, w_j, w_{ij}\}$ bound a pants patch T_k. Remove T_k from M_k: $M_k \leftarrow M_k \setminus T_k$.
  Remove w_i and w_j from W, and add w_{ij} into W.
  $k \leftarrow k + 1$.
End While

Output Set of $-\chi(M)$ pants patches $T = \{T_1, ..., T_{-\chi(M)}\}$, with $M = \cup T_i$.

pants patch the number of quadrilateral patches is set to respect sharp vertices, sharp edges and local features. That is why we talk about feature-aware cuboid decomposition $\mathbb{C}$. Figure 4 provides keys points of the proposed method. Besides, remark that curves and 4-valency nodes of $\mathbb{Q}$ are not particularly lying and sitting on features. Depending on the geometry provided by a specific pants patch, we need a precise cuboid configuration template to be mapped into the surface. This idea is illustrated in figure 5.

Finding the best cuboid configuration template for each pants patch in an automatic manner is a difficult task in the general case. In the present work, since this choice has to be done only once for the population of studied cases, we believe that it is reasonable to require the user to pick the best template available. For more details, we refer the reader to Maquart [32], chapter 3.

2.4. Direction field generation

Concept of 4-symmetry directions fields (i.e., cross fields) have been introduced previously in section 2.1. They are widely used to determine an aligned global parameterization [17, 18, 33, 34]. Designing a smooth cross field $\mathcal{C}$ is done with a given set of constraints. We categorize these constraints in two groups: topological and geometrical constraints. Topological constraints are imposed singularities and numbers induced by the surface topology $\chi(M)$. The quadrilateral layout $\mathbb{Q}$ or cuboid configuration $\mathbb{C}$ are holding these topological information. Geometrical constraints are intrinsically embedded on the surface geometry. They are given by the geometry of the surface M. In the following we seek to compute a cross field $\mathcal{C}$ which is smooth, aligned with local geometry and topologically compatible.

Discretization

Cross field discretization is based on two different approaches. *Period jump based discretization* is used for geometrical design whereas *connection angle based discretization* is used for topological design. We consider a triangulation of the surface M, assumed to be a 2-dimensional manifold of genus-g with b boundary components. Directions of the cross field $\mathcal{C}$ will be stored at faces F. We chose a local orthonormal frame $(\mathbf{x}, \mathbf{y})$ attached to each face f. If we set $\mathbf{x}$ as a unit vector along one of the oriented edges of face f, we can express $\mathbf{y} = \mathbf{n} \times \mathbf{x}$. $\mathbf{n}$ being the normal to f. We denote α the *direction angle* that makes a direction $\mathbf{u}$ on

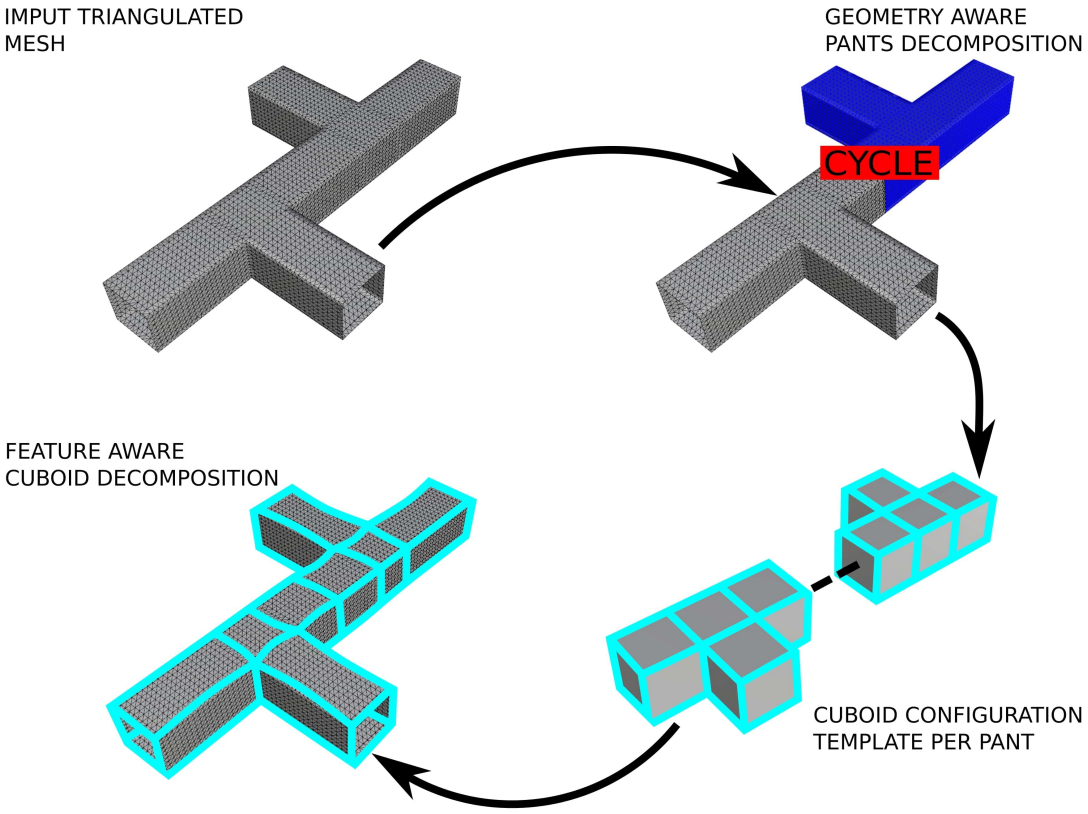

Figure 4: Smart model decomposition workflow. Starting with a triangulated surface, we decompose into a set of topological pants. Afterwards, depending on the features embedded in the input mesh, cuboid configuration templates per pant are chosen. These templates are then mapped back into the surface mesh.

a face f with the local frame. A common coordinate frame can be found by unfolding adjacent triangles isometrically to a plane along their common edge. In other words, we can formulate an angle of face f_i in f_i's adjacent faces. When walking from a face f_i to a face f_j, an infinite number of interpolation possibilities exist. This ambiguity can be solved between two points by specifying an integer p called the *period jump* [35]. This number specifies the number of N^{th} turns the direction $\mathbf{u}_A$ undergoes to match with $\mathbf{u}_B$ when passing from A to B. We introduce ${}^{p}\kappa_{\mathcal{C}}(e^*_{ij})$ as the field curvature for the *period jump based discretization* along the oriented dual edge e^*_{ij}. Other works introduce an angle w named *connection angle* to solve the ambiguity [19, 36]. As for the previous discretization, ${}^{c}\kappa_{\mathcal{C}}(e^*_{ij})$ is the field curvature for the *connection angle based discretization* along the oriented dual edge e^*_{ij}.

Smoothness design

We wish a smooth cross field $\mathcal{C}$ that is singular only at specified vertices: the position of irregular nodes of $\mathbb{Q}$. Geometrically, $\mathcal{C}$ must follow the sharp features, boundaries and relevant principal curvature directions. We want to fix all topological degrees of freedom to restrict the cross field topologically compatible to our quadrilateral layout $\mathbb{Q}$. These topological degrees of freedom are identified to be turning numbers along $2g$ homology generators, $max(b-1,0)$ boundary cycles and s singularities [20]. We use the approach of Campen and Kobbelt [17] to determine turning numbers from the input quadrilateral layout. Measuring smoothness of a cross field reduces to measuring the smoothness of one of the four directions if the toplogy is fixed. This smoothness energy can be simply calculated as its integrated squared curvature $\kappa_{\mathcal{C}}$ [20]:

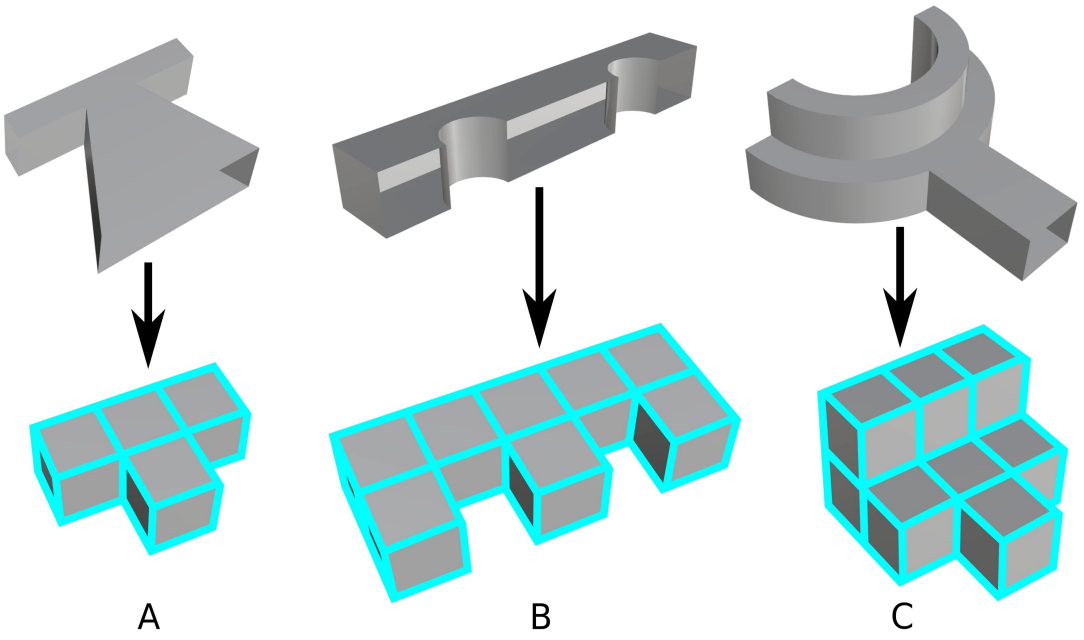

Figure 5: Cuboid configuration templates $\mathbb{C}$. To understand all the features of a CAD model, a specific cuboid configuration has to be applied for mapping purposes. (A) Represent the simplest cuboid configuration $\mathbb{C}$ for a pant. (B) Configuration $\mathbb{C}$ with 8 cuboids. (C) Configuration $\mathbb{C}$ with 10 cuboids.

$$ {}^{c}E(\mathcal{C}) = \sum_{e^*_{ij} \in E^*} \| {}^{c}\kappa_{\mathcal{C}}(e^*_{ij}) \|^2, \tag{7} $$

where E^* describes the set of dual edges. We minimize the previous energy ${}^{c}E(\mathcal{C})$ to determine the field topology using *connection angle based discretization* in equation (7). Hence the topology of the field is fixed, we now compute a smooth cross field that interpolates relevant principal curvature directions, sharp features and boundaries restricted to a given topology. We search the smoothest field taking into account constrained directions α_c contained in a subset of faces $F_c \subset F$. The period jumps of the field are fixed and the direction angles α are the only remaining variables used for the constrained optimization problem by minimizing the energy of the left member of equation (8). Using a technique presented by Bommes et al. [18], we minimize:

$$ \min_{\alpha \in \mathbb{R}^{|F|}} \sum_{e^*_{ij} \in E^*} \| {}^{p}\kappa_{\mathcal{C}}(e^*_{ij}) \|^2 = \min_{\alpha \in \mathbb{R}^{|F|}} \| \mathbf{A}\boldsymbol{\alpha} - \mathbf{b} \|^2 \text{ s.t. } \alpha_i = \alpha_c, \ \forall f_i \in F_c. \tag{8} $$

Where $\mathbf{A} \in \mathbb{R}^{|E| \times |F|}$, $\mathbf{b} \in \mathbb{R}^{|E|}$, and $\boldsymbol{\alpha} \in \mathbb{R}^{|F|}$. Remark that $\boldsymbol{\alpha} \in \mathbb{R}^{|F|}$ is the vector of unknown direction angles embedded on each face of the mesh M. Figure 6 (A) shows a geometrical cross field that interpolates boundaries whereas figure 6 (B) interpolates sharp edges. We refer the readers one more time to the work of Bommes et al. [18] for details on matrix construction.

2.5. Surface parameterization computation from direction field

Next step is done by computing an *aligned global parameterization*, i.e., a map from the mesh M to a disk-like surface parameter domain $\Omega \in \mathbb{R}^2$. We assign a couple (u, v) of parameter values on each vertex of the surface mesh M. The guiding geometrical cross field previously computed is used to align locally the

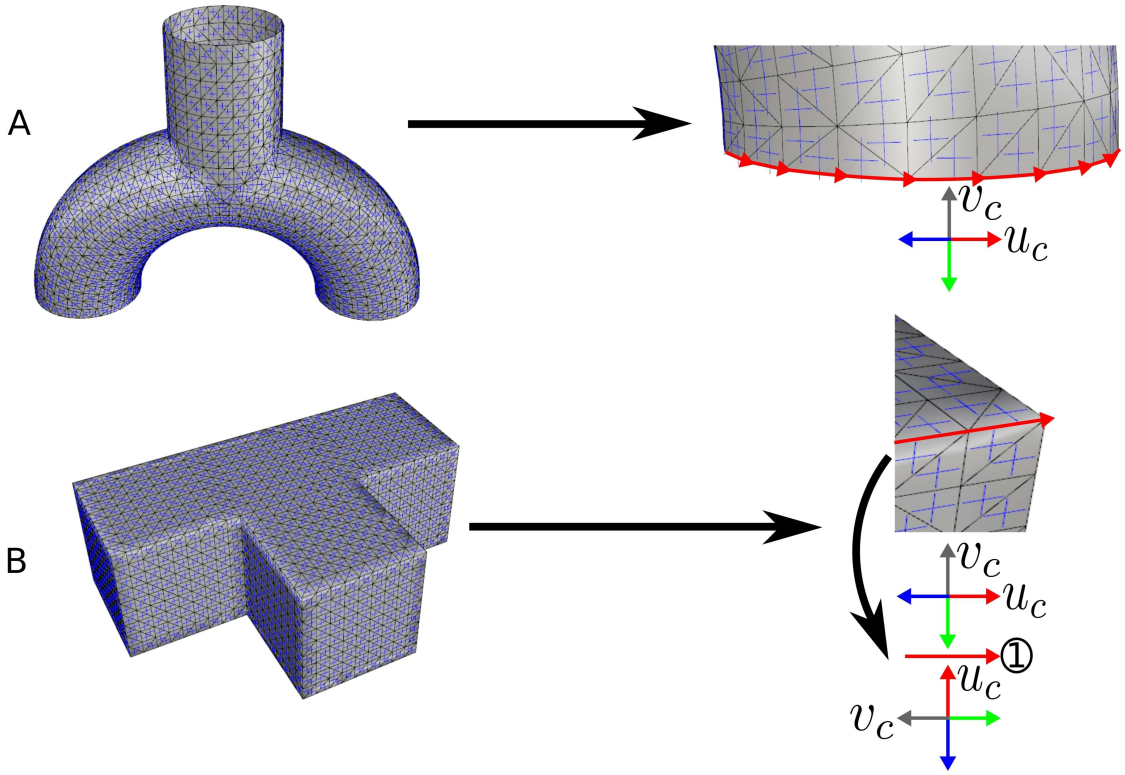

Figure 6: Direction field generation. (A) Geometrical cross field with boundary constraints. (B) Geometrical cross field with sharp edges constraints. We note a period jump of 1 along the sharp edge due to the incident sharp corner.

parameterization with the features catched by directions of the field. Such parameterization implies that the gradients ∇u and ∇v of the discrete scalar field must follow the cross field directions on each face. For that purpose we have to define a cut graph G that splits the mesh into a disk-like surface mesh M^g. Transitions across seams of the cut graph need to belong to a very restricted class. We search for rigid transformations with a rotation angle multiple of $\frac{\pi}{2}$. Moreover across each seam edge or vertex, the corresponding transition must be integral, i.e., relative to an integer. Thus we talk about integral seamless parameterization [37]. For more details about integral seamless parameteriation, we refer the readers to the work of Myles and Zorin [38] and Bommes et al. [18]. We target the cross field first and second directions $\mathbf{u}^{\mathcal{C}}$ and $\mathbf{v}^{\mathcal{C}}$ for the gradients of the parametric coordinates ∇u and ∇v. The parameterization is then computed as the solution of a constrained minimization problem [17, 18, 33]:

$$\min_{u,v} \sum_{f \in F} [\|\nabla u - \mathbf{u}^{\mathcal{C}}\|^2 + \|\nabla v - \mathbf{v}^{\mathcal{C}}\|^2] A_f \text{ s.t. equation (10)}, \tag{9}$$

where A_f is the area of the considered face f. Related additional constraints can be found here [37, 38].

In addition, with consistent quadrilateral layout and geometrical cross field provided, we wish to restrict each arc in a way that the two incident nodes lie on a common isoparametric curve where u or v are constant. We apply node connection constraint which are derived from the quadrilateral layout $\mathbb{Q}$. Typically, each arc with endpoints n_1 and n_2 must lie on a common isoparametric curve taking seams transitions into account. Thus the complete constraint has the form [39]:

$$n_{2_u} = [(\prod_{i=0}^{m} R_{(m-i)+1}) n_{1_u} + (\sum_{i=0}^{m-1} (\prod_{j=0}^{m-1-i} R_{(m-j)+1}) t_u^{i+1}) + t_u^{m+1}]. \tag{10}$$

Considering a path crossing cut edges $e_i,\ \forall i \in \{0, 1, ..., m-1, m\}$ and rotation operators $|R| = |t| = m+1$ linking node n_1 and n_2; n_{2u} is defined as the linked u parametric value from the u parametric value of n_{1u}. Thus we are able to compute a suitable global parameterization of the mesh M, given the quadrilateral layout $\mathbb{Q}$. Depending on geometry and position of $\mathbb{Q}$'s nodes, a better parameterization can be found using node relocation. The nodes are re-positionned based on the gradient of the parameterization's objective functional with respect to their positions in order to minimize the parameterization energy in equation (9). We follow the method developped by Campen and Kobbelt [17] to perform such optimization. Figure 7 (A) shows a T-part with its global parameterization optimized. Observe the final feature-comprehensive nodes and curves relocation of $\mathbb{Q}$ in figure 7 (B). The obtained final aligned global parameterization and quadrilateral layout are then used to construct a feature-aligned quadrilateral mesh depicted in figure 7 (C).

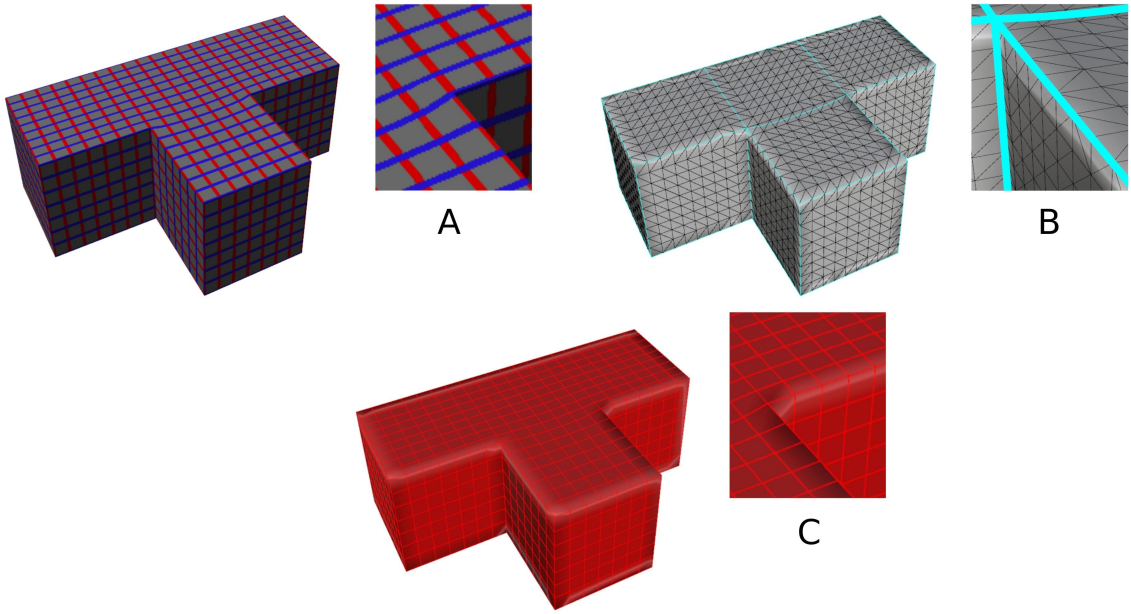

Figure 7: Surface parameterization. (A) Optimized aligned global parameterization with seam edges, and features constraints. (B) Optimized an re-positioned quadrilateral layout. (C) Feature-aligned extracted quadrilateral mesh.

2.6. Isotopological homologous 3D hexahedral meshes construction from surface parameterization

Here, we bring new useful mathematic material to convert surface parameterization into structured volumetric one. We give references to rigourous definitions and properties of topological quantities when passing in the third parametric dimension. Surface to volume conversion is a tedious task, and some properties have to be seriously analyzed to form a final valid pure hexahedral mesh. Indeed, using surface information to build a volume can lead to several different volume structures due to unset inside volume behavior. We need to identify which properties from the surface are kept into the solid and how the internal volume structure is built.

For clarity, we refer the reader to Maquart [32], chapter 6, and in particular to Maquart et al. [40]. These references explain in detail how to convert a quadrilateral layout $\mathbb{Q}$ to a closed cuboid configuration $\mathbb{C}_c$. $\mathbb{C}_c$ is then used to determine a volumetric layout $V_{\mathbb{C}}$. $V_{\mathbb{C}}$ can be viewed as a coarse hexahedral mesh whose boundary (interpreted as a surface) is topologically equivalent to the input unstructured triangulated mesh without boundaries.

2.6.1. Volumetric parameterization

With a valid closed cuboid configuration $\mathbb{C}_c$ that will describe a volumetric layout $V_{\mathbb{C}}$ satisfying previous topological properties from Maquart et al. [40], we are able to construct a volumetric parameterization. First, we take the quadrilateral mesh extracted from the optimized aligned global parameterization. This quadrilateral mesh can be viewed as a set ordered points. We use the software Rhinoceros 5 [41] to fit B-Spline surfaces with this specific point grids. We manipulate compatibility and patch refinement with the Rhinoceros software library [42]. Secondly, for each cuboid, the B-Spline solid is obtained using reconstructed B-Spline boundary surface as boundary conditions. The positions of the interior control points of the solid are calculated in a way to minimize the Laplacian based energy. We follow in particular the work of Wang and Qian [43] for that purpose. Figure 8 illustrates the method for trivariate isogeometric reconstruction from closed cuboid configuration $\mathbb{C}_c$.

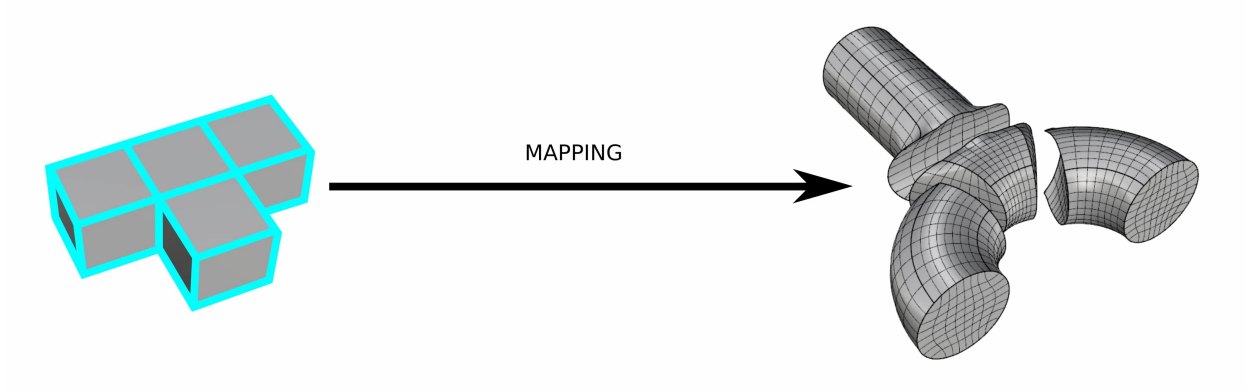

Figure 8: Volumetric isogeometric parameterization. Using a valid closed cuboid configuration $\mathbb{C}_c$ that forms a volumetric layout $V_{\mathbb{C}}$, this configuration is then mapped into a topologically and geometrically compatible B-Rep. Aligned global parameterization is computed and B-Spline surfaces are fitted. Due to the volumetric layout properties inherited from $\mathbb{C}_c$, trivariate isogeometric parameterization is deducted.

2.6.2. Isotopological constraints for volumetric parameterization

Understanding significance of above developments, we reformulate here the problematic exposed in section 1. Given a set of input triangulated meshes, we strive to find an isotopological trivariate isogeometric meshes population which respect the four following properties:

- Pure hexahedrons with low distortion for the trivariate control lattice.
- Feature aligned with geometry inherited from the triangulated surface.
- Isotopological with homologous points into other geometric instances.
- Non-uniform *isotropy* for a morphing to all members of the population.

To build isotopological meshes for a specific set of related meshes, the discretization sampling is based on one representative member of the population. We call him the *α-member*. Taking into account features and geometry of the *α-member* mesh, isotopological and homologous constraints are then settled for all members. Non-uniform *isotropy* is therefore intrinsically set because of volume number, connectivity and discretization.

3. Application to reduced order modeling with geometric parameters

Our algorithm is entirely incorporated into a Rhinoceros 5 [41] Plug-In implemented in VB.NET. C++ processes are called from the Plug-In. Some prerequisites are mandatory, such as a consistent pants-to-cuboids decomposition. We use for that purpose the ROM (Reduced Order Model) builder proprietary

software developed by ANSYS [44]. This ROM solution works using classical Singular Value Decomposition algorithms [45, 46]. Response surfaces reconstruction are made with standard kriging tools. Figure 9 gives the standard principle of operation. Recently, this builder has been used to prevent excessive compression of buttock's soft tissues by bony structures in real-time for paraplegic persons [47].

Many modern numerical models of real-life physics computations pose challenges when used in numerical simulations, due to time complexity and large size. As a consequence, novel methods are required in order to tackle not only non-linear problems but also large scale and parametric problems. This is the principal motivation behind reduced order modeling. This method enables real-time analysis due to its very low computational cost during evaluation. The construction of different geometrical parametric studies requires in general a set of geometries with specific properties. These geometries coupled with material or physical parameters are called snapshots. Isotopological and homologous meshes are required for reduced order modeling with geometrical parameters to avoid an inaccurate projection step. We use in the following the so-presented MEG-IsoHex method to obtain such properties of meshes.

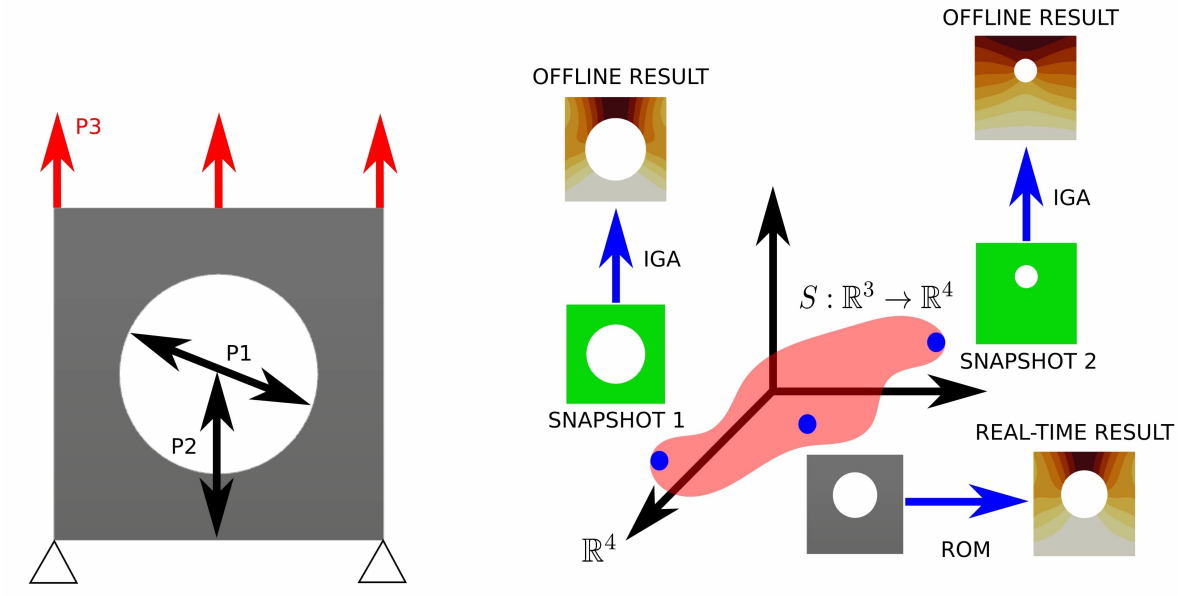

Figure 9: Reduced order model building and evaluation for a plate with one hole. Snapshots are calculated using IGA (IsoGeometric Analysis). $P1$ and $P2$ are geometrical parameters defining respectively the diameter and the position of the hole along his height. $P3$ is a loading parameter. Response surfaces S are embedded in 4-dimensional space. There are as many surfaces as there are modes in the reduced basis.

3.1. Isotopological hexahedral remeshing for large deformations

In this section, we study the use of our algorithms to perform the isotopological remeshing during a hyperelastic simulation. Although no reduced order modeling is introduced in this example, hyperelastic large strain calculation is a case in which classical *a posteriori* reduced order models are not efficient because of the needed remeshing during the calculation of a given snapshot. Indeed when high strains are encountered, standard finite element meshes often lead to poor element shapes during the computation, and remeshing is unavoidable to be able to perform the simulation until the end. As for geometric parametric studies, the use of isotopological meshes is required for ROM algorithm to perform efficiently when remeshing is needed.

In this example, we consider a simple compressible Neo-Hookean material, see e.g. Simo and Hughes [48], Lemaitre and Chaboche [49], and use our mesh generation algorithms on a half-seal part composed by one pants patch as presented in figure 10. For this particular case, we consider degree 1 B-Splines which are nothing more than standard piecewise linear hexahedrons classically used in FEA. The same parameters

(cuboid configuration, singular points, number of nodes and connectivity) will be used to remesh a deformed configuration of the model at a given intermediate time of the simulation. The input mesh and boundary conditions are given in figure 11 (A). We consider a quasi static computation with a ramp loading from $t = 0$ to $t = 1$ and use the following values for the material parameters: $\mu = 3$ MPa and $\kappa = 20$ MPa for the shear and bulk modulus respectively. These material parameters imply a Poisson's ratio equal to $\nu = 0.3636$, which corresponds to a compressible material. The finite element calculation is classically performed using a total Lagrangian approach, again see e.g. Simo and Hughes [48]. Based on the results of the full calculation without remeshing, we observe that element quality metrics of the deformed mesh start to deteriorate significantly after $t = 0.5$. Consequently, we extract the deformed geometry at this particular time and use our algorithms to create a new isotopological mesh to improve element aspect ratio and overall quality. The new mesh used form $t = 0.5$ can be seen in figure 11 (A). In order to evaluate mesh quality, we use as a metric the element shape ratio S_r classically available in commercial softwares such as ANSYS. $S_r = \frac{A}{B}$ measures the stretching of the element, where A is the maximum distance from the hexahedral centroid to one of the eight corners and B is computed as the minimum value of the normal distance between the cell centroid and face centroids (computed as a dot product of the distance vector and the face normal). Therefore, for a unit cube we have $S_r = 1.732$.

In our calculation with remeshing, once we have created the new mesh with the MEG-IsoHex strategy, the displacement field is mapped from the old to the new mesh using standard techniques. The finite element calculation is resumed by considering an initial deformation state computed using the deformation gradient after projection onto the new mesh.

Element shape ratio computed at $t = 0.5$ and $t = 1$ on both meshes are shown in figures 11 (B) and (C). We can observe that at $t = 0.5$ the remeshing reduces the maximum value of S_r by approximately 30%. A similar observation can be done at the final time $t = 1$, where the element shape ratio is even further reduced compared to the simulation with the initial mesh. We also compare the Von-Mises stresses at the final time for both cases to check that the remeshing and mapping steps lead to the correct solution. Figure 12 shows the corresponding results for the unremeshed case (A) and remeshed case (B). For visualisation and comparison purposes, we build an associated linear hexahedral element mesh whose geometry is described by the Gauss points of the underlying FE mesh. We can see that for both cases the closest Gauss point near the corner have very similar Von-Mises stress values, in the same difference range as can be observed by comparing simulation results using commercial FE packages such as ANSYS and ABAQUS for the same example with the same mesh density.

These results clearly show the efficient of our method to improve the mesh quality during a highly deformed hyperelastic simulation while preserving correctness of the finite element solution.

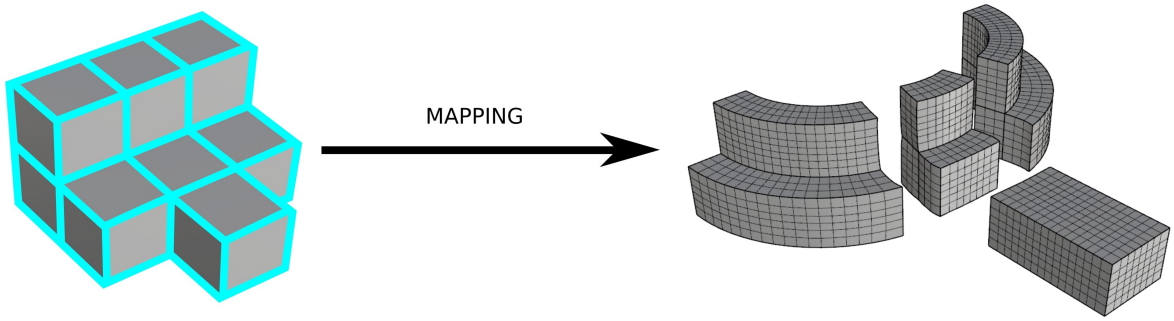

Figure 10: Volumetric isogeometric parameterization of the half-seal part for remeshing purposes. It is a genus-0 geometry with sharp features. Euler characteristic is $\chi = -1$ for the mesh with 3 specific boundaries. During the remeshing step, the parameterization is still the same whereas the geometry is changing under loading.

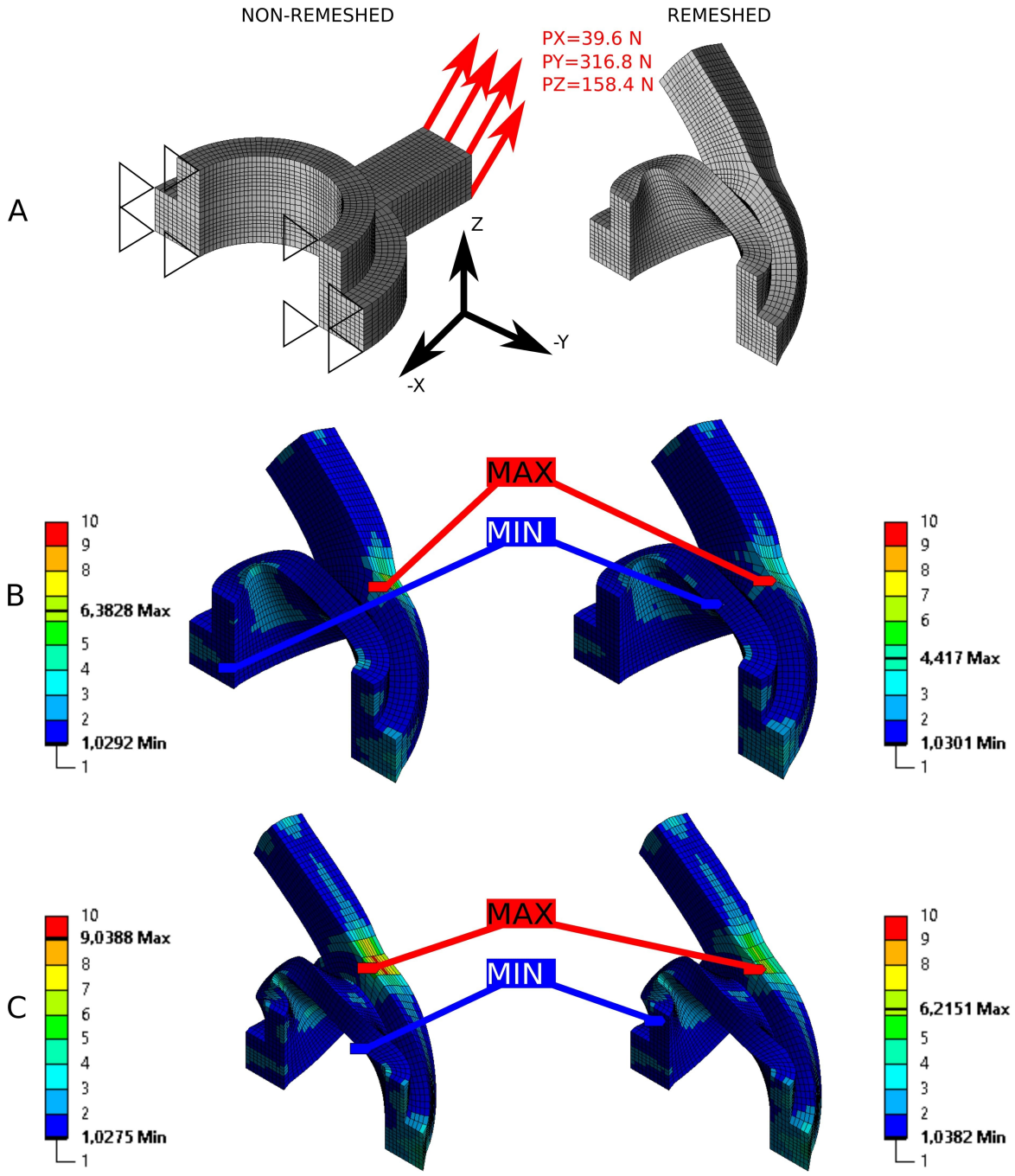

Figure 11: Element quality comparison under loading for the half-seal part. (A) The initial mesh at $t = 0$ with boundary conditions (left). The remeshed case at $t = 0.5$ (right). (B) Element shape ratio at $t = 0.5$ without remeshing process (left). Element shape ratio at $t = 0.5$ with remeshing process (right). (C) Element shape ratio at the last loading increment without remeshing process, $t = 1$ (left). Element shape ratio at the last loading increment with remeshing process, $t = 1$ (right). All deformed shapes are given with a scale factor of 1.

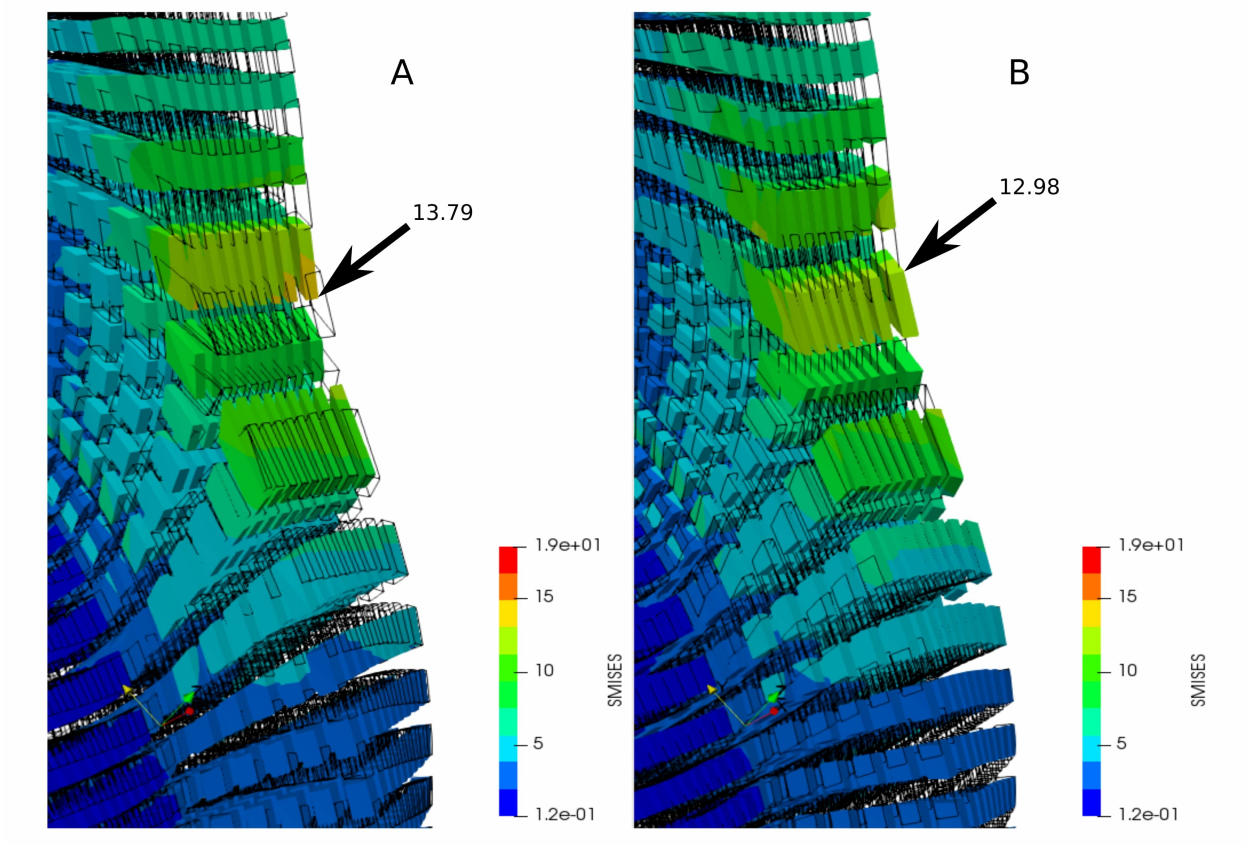

Figure 12: Details of Von-Mises stress comparison at Gauss points. For each hexahedral element, we build an associated linear hexahedral element which geometry is described by its related Gauss points. (A) Stress for the unremeshed case at $t = 1$. Elements made by Gauss points of the remeshed part are depicted in black wireframe. (B) Stress for the remeshed case at $t = 1$. Elements made by Gauss points of the unremeshed part are depicted in black wireframe.

3.2. Isogeometric reduced order models

In this section we deal with two examples of reduced order models. We organize this section flow in three main parts. First, we give graphical data based on above advances to construct isotopological homologous meshes for snapshots. To compute the mechanical fields for our snapshots, we use isogeometric analysis [6, 31, 50, 51] to solve a linear elastic problem. In a second time, we develop the sampling of parameters for very-large parameter spaces. To finish, evaluations of the reduced order models built are depicted.

Using our technique of pants-to-cuboid decomposition understanding features of input triangulated meshes, a cuboid configuration $\mathbb{C}_c$ template is associated to each pant composing the B-Rep surface geometry. Aligned global parameterization is computed and boundary B-Spline surfaces are fitted. We then extract a volumetric parameterization of our input geometries due to the properties of the volumetric layout $V_{\mathbb{C}}$. A very simplified workflow is decribed in figures 13 for the seal and 14 for the wheel part. This is done among all different geometrical snaphsots of the population taking a *α-member* as reference. As said in section 2.6.2, to build isotopological meshes for a specific set of related meshes, we use one representative member of the population called the *α-member*.

Sampling of parameters have been done using a sparse grid technique [8, 52, 53]. Adopting this method in a low level manner, i.e., by populating only axis of parameters, we are then able to fill large parameter spaces. Indeed, sparse grids are especially more suitable for high-dimensional problems. A sparse grid method to sample snapshots among a large parameter space is an efficient solution for a fast *a posteriori* learning strategy. However, for high-dimensional problems such as the ones we are studying, a larger amount

of relevant snapshots is required. For each isotopological geometry, for each loading parameter and then for each mechanical property a snapshot is produced and solved using IGA. Range of parameters and sampling along parameters axis refer to the sparse grid technique with the existence of a hypercenter of the n-dimensional problem.

Seal part reduced order model is constructed taking 400 snapshots. The model holds 6 geometrical parameters, 1 loading parameter and 1 mechanical parameter as described in figure 15. G refer to the number of different isotopological geometries, P to the number of loading cases and M is the number of material parameters. Equation (11) shows the distribution of parameters in a tensorial form between the 3 different quantities.

$$\dim(G \otimes P \otimes M) = \dim(G) \times \dim(P) \times \dim(M) = 25 \times 4 \times 4 = 400. \tag{11}$$

With the same idea, the wheel part is built with 592 snapshots. 9 geometrical parameters are being considered. Figure 15 and equation (12) explain the attribution of parameters.

$$\dim(G \otimes P \otimes M) = \dim(G) \times \dim(P) \times \dim(M) = 37 \times 4 \times 4 = 592. \tag{12}$$

Snapshot production is done by considering a standard B-Rep CAD as input. Depending on the triangle discretization of the CAD geometry, our segmentation algorithms such as the pants-to-cuboids decomposition take a reasonable computing time. For the examples detailed in the current work, few minutes are required per snapshot evaluation.

ROM evaluation is done in near real-time: few seconds are necessary. Examples of such fast solution computation are depicted in figure 17 for the seal part and 18 for the half part. Each evaluation were done involving a random set of parameters. A couple of seconds are needed to obtain the displacement magnitude. Thanks to isotopological meshes, we have introduced many geometrical parameters into the learning process. Results are shown for geometrical virtual charts that can be used for shape optimization or an industrial sizing purpose. Moreover, accuracy of evaluations are improved due to the availibility of isotopological homologous meshes. Indeed, data embedded on structured meshes are really appreciated in comparing mechanical fields. Projection steps are thus avoided. This is done by constraining the parameterization among all meshes composing the population to be reduced. In addition, homologous concepts allow to compare information at the same location, i.e., in a the same relevant geometry zone for all geometrical instances.

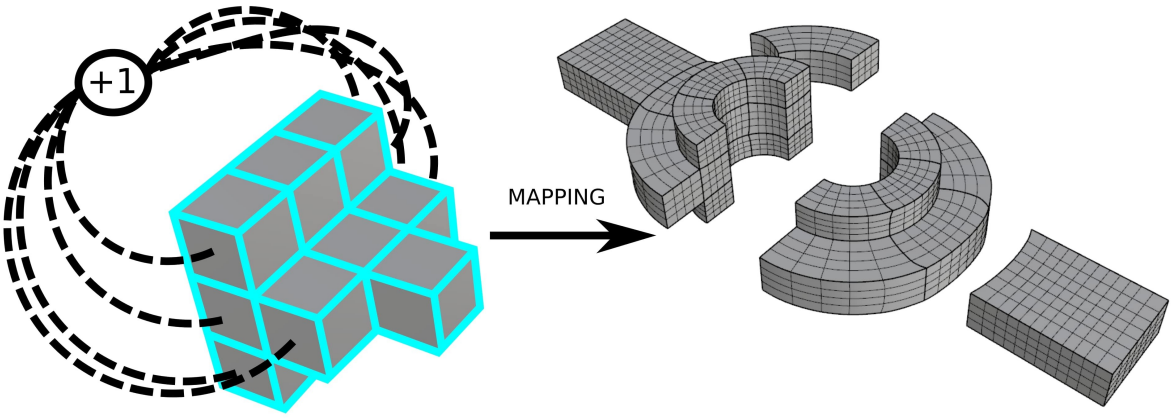

Figure 13: Volumetric isogeometric parameterization of the seal part. It is a genus-1 geometry with sharp features. Euler characteristic is $\chi = 0$ for the associated closed mesh M_c. We apply the same parameterization among all members of the population to obtain isotopological comparable isogeometric meshes.

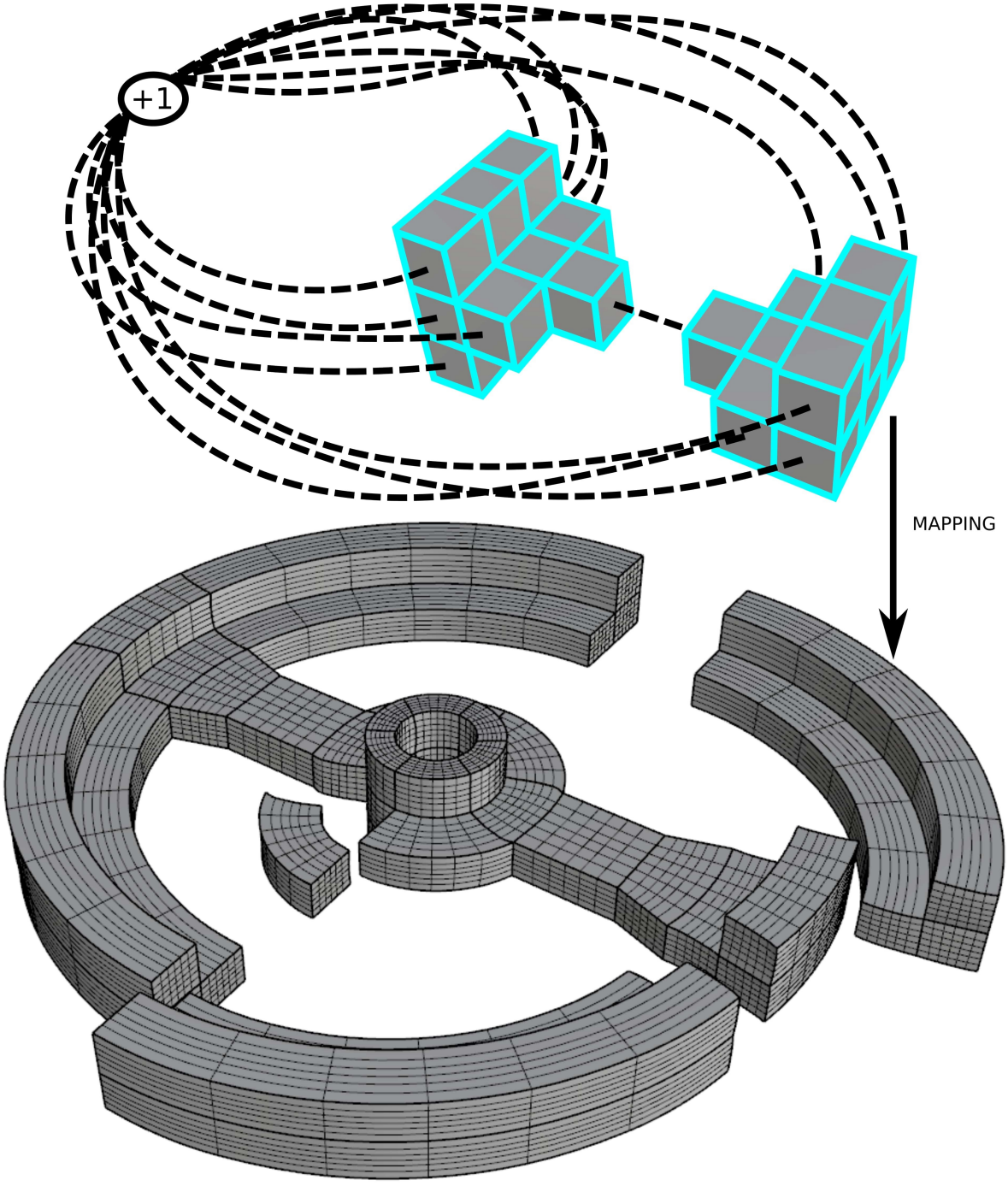

Figure 14: Volumetric isogeometric parameterization of the wheel part. It is a complex genus-3 geometry with sharp features. Euler characteristic is equal to $\chi = -4$, involving a decomposition in 4 pants. We apply the same parameterization among all members of the population to obtain isotopological comparable isogeometric meshes.

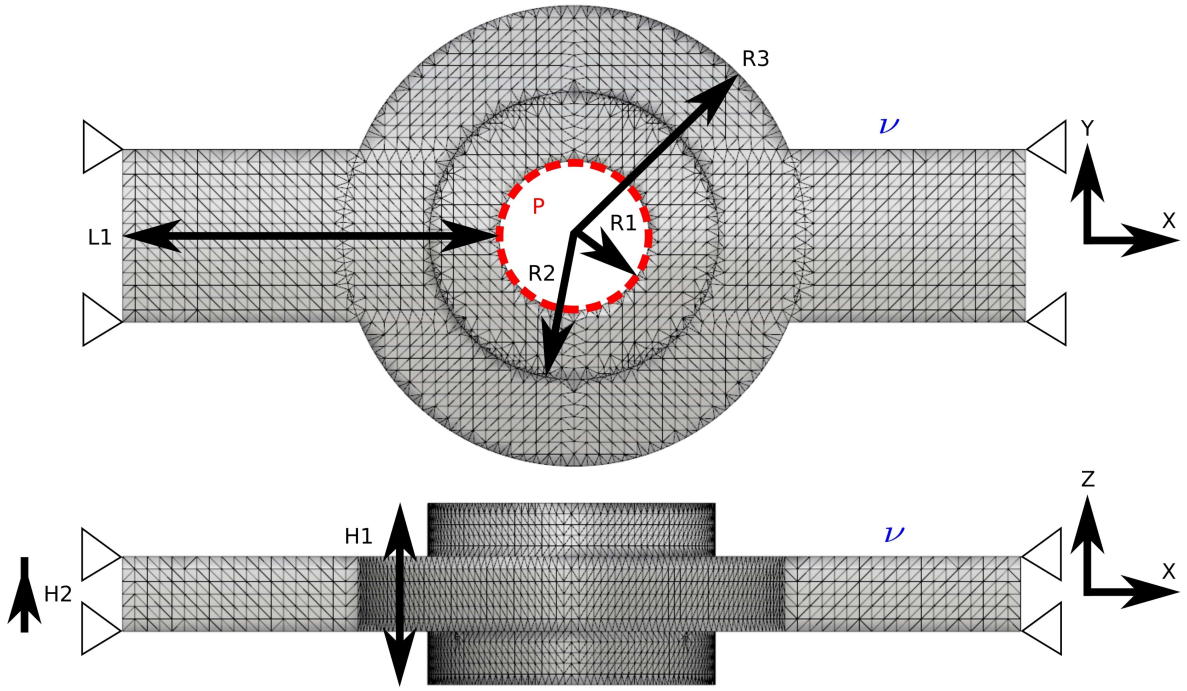

Figure 15: Seal part distribution of parameters. 6 geometrical parameters are settled. 1 load parameter P is applied and poisson's ratio ν is devoted to be a mechanical parameter. We use a constant Young's modulus $E = 210$ GPa. Loads and boundary conditions are distributed on concerned nodes.

Seal part range	Min	Max
Radius 1	11	15
Radius 2	20	30
Radius 3	35	45
Height 1	28	35
Height 2	10	16
Length 1	50	80
Load intensity	100 N	175 N
Poisson's ratio	0.28	0.34

Wheel part range	Min	Max
Radius 1	7.8	9.75
Radius 2	13.65	16.25
Radius 3	25.35	29.9
Radius 4	62.725	67.275
Radius 5	73.775	80.275
Radius 6	86.625	91.975
Height 1	26	32.5
Height 2	8.125	9.75
Length 1	39	43.875
Load intensity	100 N	175 N
Young's modulus	200 GPa	230 GPa

Table 1: Range of parameters used for the seal and wheel part reduced order models.

4. Conclusion

We have introduced in this paper a volumetric isotopological mesh generation method from B-Rep CAD. We have shown that our meshing strategy is well-suitable for reduced order modeling with geometric parameters. Comparing mechanical fields efficiently is done by adressing the same parameterization of different geometrical instances. In fact, avoiding a projection step and setting homologous parameterizations yield to accurate reduced order models. Moreover, introducing geometrical parameters into a reduced order model enables shape optimization that is useful nowadays in a part weight reduction objective. A real

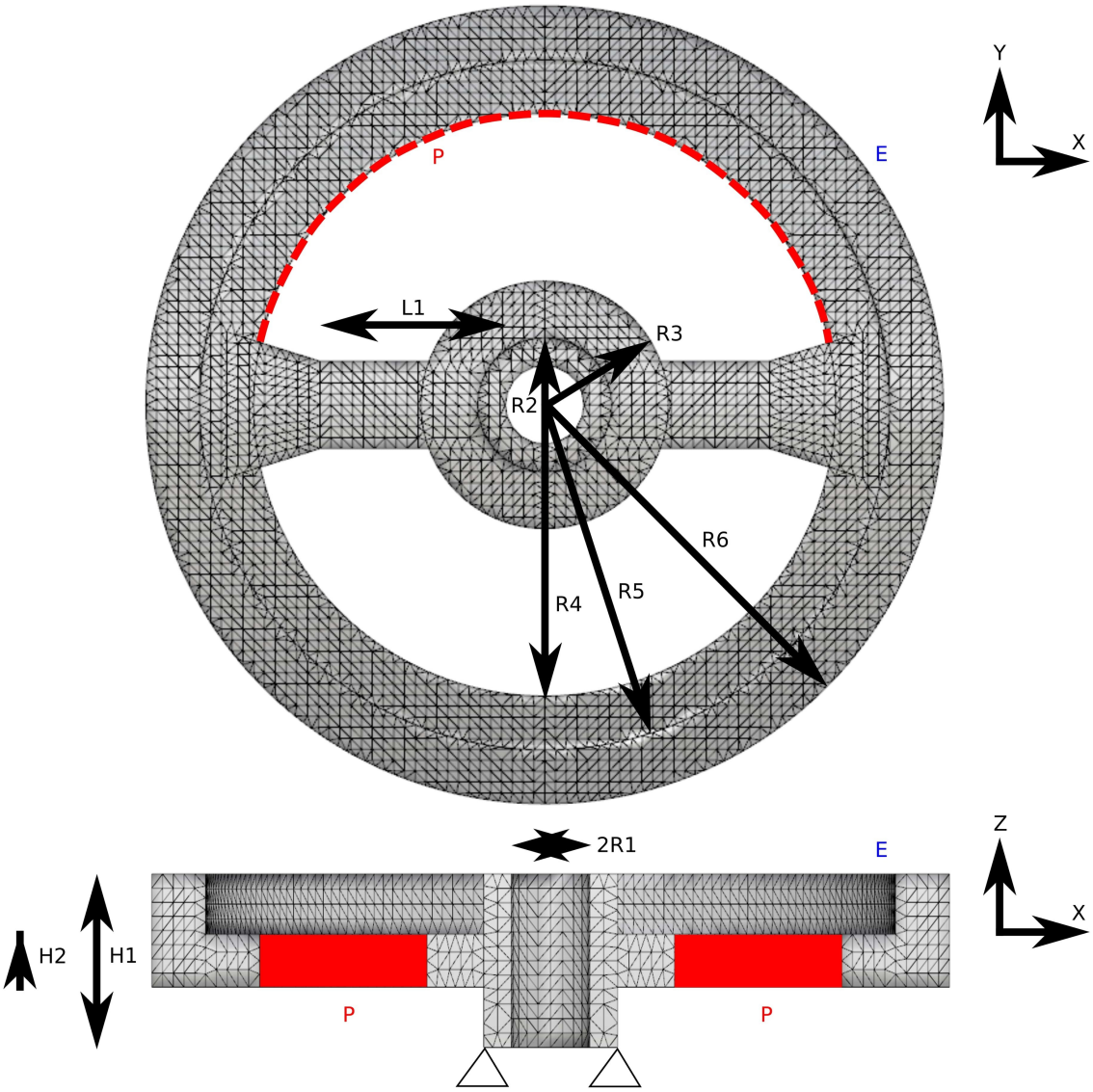

Figure 16: Wheel part distribution of parameters. 9 geometrical parameters are settled. 1 load parameter P is applied and Young's modulus E is devoted to be a mechanical parameter. We use a constant poisson's ratio $\nu = 0.3$. Loads and boundary conditions are distributed on concerned nodes.

benefit has been deployed by defining a generic method to overcome the unavailability of isotopological meshes. MEG-IsoHex method was introduced to solve the problem in a universal form. This helps us to define a set of 3D volumetric isotopological homologous meshes. Presented real-time evaluations demonstrate the robustness and the reliability of the developed method.

A first key contribution is done in the segmentation of the input surface provided by the CAD. Surface decomposition theory is an essential tool to fulfill our objectives. We strive to understand both geometry and topology during this step. A second improvement is to position the singularities in the best possible way. Gaussian curvature distribution is naturally defined to locate them if curvature is sampled in few vertices on the mesh. For other properties like singularity indices, field turning numbers and surface global parameterization, we have used the work of Campen and Kobbelt [17] coupled with our previous

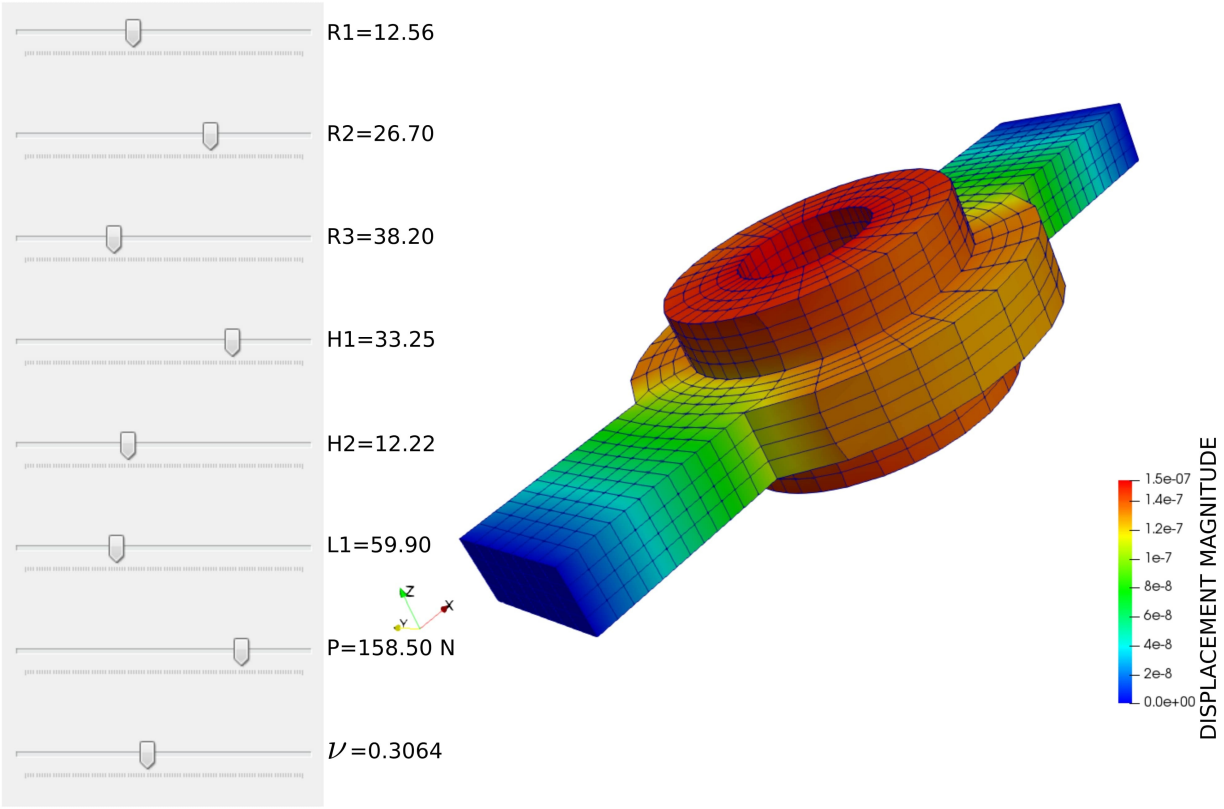

Figure 17: Seal reduced order model real-time evaluation. A 9-dimensional manifold built by kriging tools is evaluated to find preponderant coefficients attached to the first 50 modes. Isogeometric elements are sampled with one hexahedron per element for viewing purposes in Paraview. Used range of parameters is detailed in table 1.

improvements.

We gave new mathematical tools to understand properties during surface to volume conversion into a third significant advance. Such hard conversion problematic continues to find a certain interest in geometry processing, mechanical and physics communities. We have shown that controling topological properties during the conversion process is fundamental. Indeed, topology and mathematical features of manifolds have to be considered at the highest level. Invariant information transmitted from the surface to the volume is essential to build volumetric meshes needed by our method.

Despite the abilities of our algorithms and tools introduced in this paper, treating any arbitrary and complex CAD geometry automatically is still a challenge. For complex cases with an arbitrary geometry, pants decomposition can be not consistent. It can be solved by adding user proposals into the automatic process. Generated quadrilateral layout is adapted to surface definition resulting in an arbitrary definition of the interior volume. But, it can be tackled by addressing specific user input information to the workflow.

5. Acknowledgments

T. Maquart was partially supported by a CIFRE fellowship of the french Association Nationale de la Recherche et de la Technologie and ANSYS research. T. Maquart, T. Elguedj and A. Gravouil were also partially supported by a research contract with ANSYS. These supports are gratefully acknowledged. All the reduced order model computations are performed with the reduced order model builder developed by the ANSYS France research team.

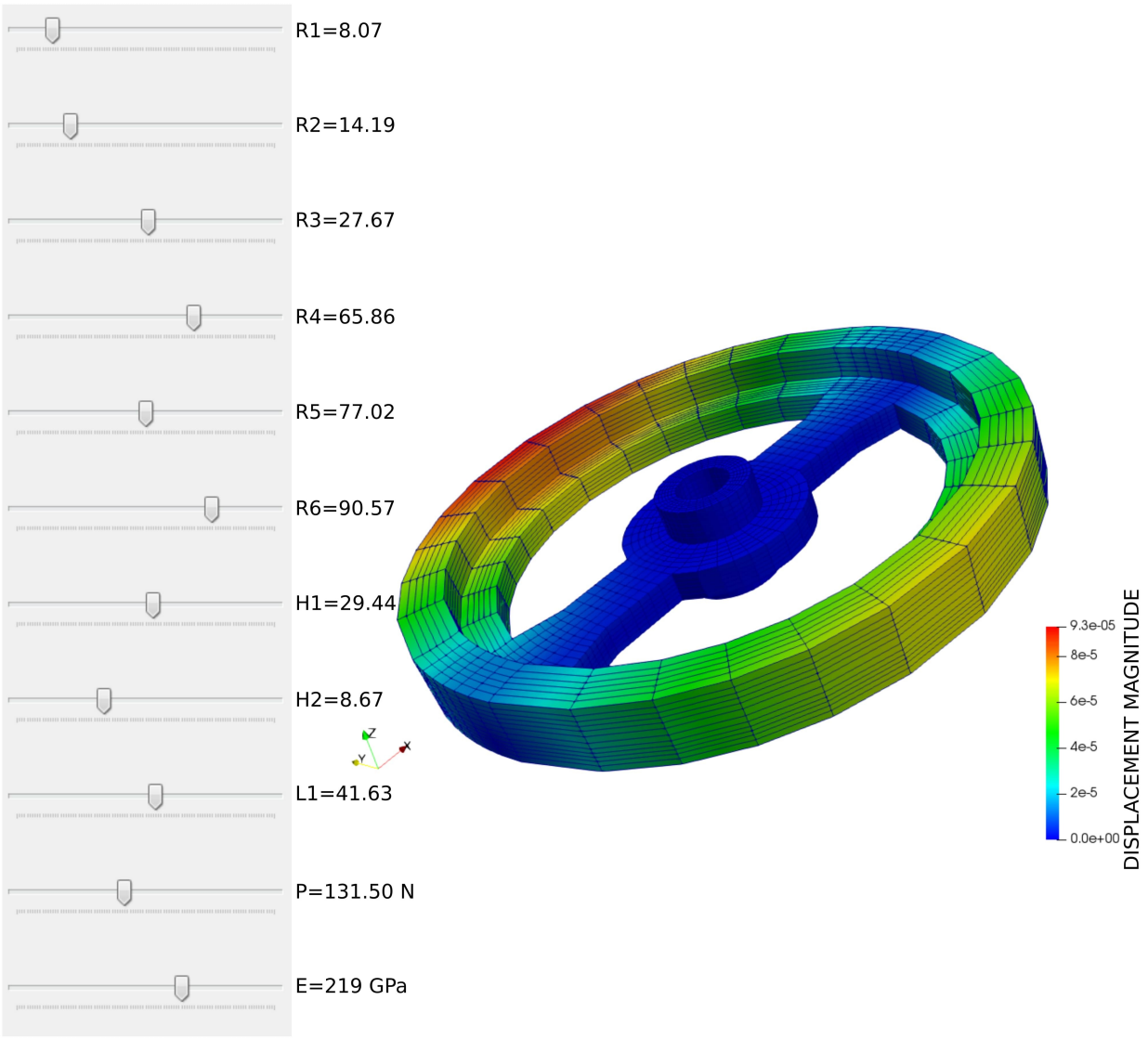

Figure 18: Wheel reduced order model real-time evaluation. A 11-dimensional manifold built by kriging tools is evaluated to find preponderant coefficients attached to the first 50 modes. Isogeometric elements are sampled with one hexahedron per element for viewing purposes in Paraview. Used range of parameters is detailed in table 1.

References

[1] F. Chinesta, A. Ammar, E. Cueto, Recent advances and new challenges in the use of the proper generalized decomposition for solving multidimensional models, Archives of Computational methods in Engineering 17 (4) (2010) 327–350.

[2] F. Chinesta, P. Ladeveze, E. Cueto, A short review on model order reduction based on proper generalized decomposition, Archives of Computational Methods in Engineering 18 (4) (2011) 395.

[3] S. Niroomandi, I. Alfaro, E. Cueto, F. Chinesta, Real-time deformable models of non-linear tissues by model reduction techniques, Computer methods and programs in biomedicine 91 (3) (2008) 223–231.

[4] A. Courard, D. Néron, P. Ladevèze, L. Ballere, Integration of PGD-virtual charts into an engineering design process, Computational Mechanics 57 (4) (2016) 637–651.

[5] T. Hirschler, R. Bouclier, A. Duval, T. Elguedj, J. Morlier, Isogeometric sizing and shape optimization of thin structures with a solid-shell approach, Structural and Multidisciplinary Optimization (2018) –.

[6] J. A. Cottrell, T. J. Hughes, Y. Bazilevs, Isogeometric analysis: toward integration of CAD and FEA, John Wiley & Sons, 2009.

[7] F. Galland, A. Gravouil, E. Malvesin, M. Rochette, A global model reduction approach for 3D fatigue crack growth with confined plasticity, Computer Methods in Applied Mechanics and Engineering 200 (5) (2011) 699–716.
[8] Y. Lu, N. Blal, A. Gravouil, Adaptive sparse grid based HOPGD: Toward a nonintrusive strategy for constructing space-time welding computational vademecum, International Journal for Numerical Methods in Engineering 114 (13) (2018) 1438–1461.
[9] A. Courard, PGD-Abaques virtuels pour l'optimisation géométrique des structures, Ph.D. thesis, Université Paris-Saclay, 2016.
[10] K. Zhang, X. Li, Searching Geometry-aware Pants Decomposition in Different Isotopy Classes, Geometry, Imaging, and Computing, Vol. 1, No. 3 (2014) 367–393.
[11] M. Hajij, T. K. Dey, X. Li, Segmenting a Surface Mesh into Pants Using Morse Theory, arXiv.org arXiv:1608.06368v2.
[12] X. Li, X. Gu, H. Qin, Surface Mapping Using Consistent Pants Decomposition, IEEE Transactions on Visualization and Computer Graphics 15 (4) (2009) 558–571, ISSN 1077-2626, doi:http://dx.doi.org/10.1109/TVCG.2008.200.
[13] É. Colin de Verdière, F. Lazarus, Optimal pants decompositions and shortest homotopic cycles on an orientable surface, Journal of the ACM 54 (4) (2007) Article No. 18, a conference version appeared in *Proc. Int. Symp. on Graph Drawing (GD)*, 2003. A preliminary version appeared in *Abstr. Europ. Workshop on Computational Geometry (EuroCG)*, 2003.
[14] J. Lin, X. Jin, Z. Fan, C. C. L. Wang, Automatic PolyCube-Maps, Advances in Geometric Modeling and Processing (2008) 3–16.
[15] L. Liu, Y. Zhang, Y. Liu, W. Wang, Feature-preserving T-mesh construction using skeleton-based polycubes, Computer-Aided Design 58 (2015) 162–172.
[16] B. Li, X. Li, K. Wang, H. Qin, Surface Mesh to Volumetric Spline Conversion with Generalized Poly-cubes, IEEE Transactions on Visualization and Computer Graphics 99 (PrePrints) (2013) 1, ISSN 1077-2626, doi: http://doi.ieeecomputersociety.org/10.1109/TVCG.2012.177.
[17] M. Campen, L. Kobbelt, Quad layout embedding via aligned parameterization, in: Computer Graphics Forum, vol. 33, Wiley Online Library, 69–81, 2014.
[18] D. Bommes, H. Zimmer, L. Kobbelt, Mixed-integer quadrangulation, ACM Transactions On Graphics (TOG) 28 (3) (2009) 77.
[19] K. Crane, M. Desbrun, P. Schröder, Trivial Connections on Discrete Surfaces, Computer Graphics Forum (SGP) 29 (5) (2010) 1525–1533.
[20] N. Ray, B. Vallet, W. C. Li, B. Lévy, N-symmetry direction field design, ACM Transactions on Graphics (TOG) 27 (2) (2008) 10.
[21] A. Hatcher, Algebraic Topology, http://www.math.cornell.edu/ hatcher .
[22] J. Erickson, K. Whittlesey, Greedy optimal homotopy and homology generators, 16th Annual ACM-SIAM Symposium on Discrete Algorithms (2005) 1038–1046.
[23] A. Hatcher, P. Lochak, L. Schneps, On the teichmüller tower of mapping class groups, Journal Für Die Reine Und Angewandte Mathematik 521 (2000) 1–24.
[24] T. K. Dey, J. Sun, Y. Wang, Approximating Cycles in a Shortest Basis of the First Homology Group from Point Data, ACM 26th Annual Symposium on Computational Geometry (2010) 166–175.
[25] B. Jubin, A generalized Poincaré-Hopf index theorem, arXiv preprint arXiv:0903.0697 (2009) .
[26] L. Saboret, P. Alliez, B. Lévy, Triangulated Surface Mesh Parameterization, in: CGAL User and Reference Manual, CGAL Editorial Board, 4.9 edn., 2016.
[27] W. T. Tutte, How to draw a graph, Proc. London Math. Soc 13 (3) (1963) 743–768.
[28] M. S. Floater, Mean value coordinates, Computer Aided Geometric Design 20 (2003) 19–27.
[29] T. K. Dey, K. Li, J. Sun, D. Cohen-Steiner, Computing geometry-aware handle and tunnel loops in 3D models, ACM Transactions on Graphics (TOG) 27 (3) (2008) 45.
[30] H. Al-Akhras, Automatic Isogeometric Analysis Suitable Trivariate Models Generation - Application to Reduced Order Modeling, Ph.D. thesis, INSA de LYON, École Doctorale MEGA ED 162, 2016.
[31] H. Al-Akhras, T. Elguedj, A. Gravouil, M. Rochette, Towards an automatic isogeometric analysis suitable trivariate models generation – Application to geometric parametric analysis, Computer Methods in Applied Mechanics and Engineering 316 (2017) 623–645.
[32] T. Maquart, Trivariate models generation from unstructured surface manifolds for isogeometric analysis - application to reduced order modeling with geometric parameters, Ph.D. thesis, Université de Lyon, INSA de LYON, École Doctorale MEGA ED162, 2019.
[33] D. Bommes, M. Campen, H.-C. Ebke, P. Alliez, L. Kobbelt, Integer-grid maps for reliable quad meshing, ACM Transactions on Graphics (TOG) 32 (4) (2013) 98.
[34] A. Myles, D. Zorin, Controlled-distortion constrained global parametrization, ACM Transactions on Graphics (TOG) 32 (4) (2013) 105.
[35] W.-C. Li, B. Vallet, N. Ray, B. Levy, Representing higher-order singularities in vector fields on piecewise linear surfaces, IEEE Transactions on Visualization and Computer Graphics (2006) 12 (5).
[36] K. Crane, Discrete connections for geometry processing, Master's thesis, California Institute of Technology, http://resolver.caltech.edu/CaltechTHESIS:05282010-102307125, 2010.
[37] F. Kälberer, M. Nieser, K. Polthier, QuadCover-Surface Parameterization using Branched Coverings, in: Computer Graphics Forum, vol. 26, Wiley Online Library, 375–384, 2007.
[38] A. Myles, D. Zorin, Global parametrization by incremental flattening, ACM Transactions on Graphics (TOG) 31 (4) (2012) 109.
[39] A. Myles, N. Pietroni, D. Kovacs, D. Zorin, Feature-aligned T-meshes, in: ACM Transactions on Graphics (TOG), vol. 29,

ACM, 117, 2010.
[40] T. Maquart, T. Elguedj, A. Gravouil, M. Rochette, A note on topological properties of volumes constructed from surfaces, HAL: https://hal.archives-ouvertes.fr/hal-02318094, (2019) .
[41] R. McNeel, Rhinocéros 5 3D, https://www.rhino3d.com/, 2017, 2017.
[42] R. McNeel, Rhinocommon DLL Documentation, https://developer.rhino3d.com/api/, 2017, 2017.
[43] X. Wang, X. Qian, An optimization approach for constructing trivariate B-spline solids, Computer-Aided Design 46 (2014) 179–191.
[44] Reduced order model builder (non-official title) by ANSYS, Inc., U.S. patent application 16/253,635, filed 2019-01-22.
[45] A. Giacoma, Efficient acceleration techniques for nonlinear analysis of structures with frictional contact, Ph.D. thesis, INSA de Lyon, 2014.
[46] F. Galland, An adaptive model reduction approach for 3D fatigue crack growth in small scale yielding conditions, Ph.D. thesis, INSA de Lyon, 2011.
[47] V. Luboz, M. Bailet, C. B. Grivot, M. Rochette, B. Diot, M. Bucki, Y. Payan, Personalized modeling for real-time pressure ulcer prevention in sitting posture, Journal of tissue viability 27 (1) (2018) 54–58.
[48] J. C. Simo, T. J. Hughes, Computational inelasticity, Springer Science & Business Media, 2006.
[49] J. Lemaitre, J.-L. Chaboche, Mechanics of solid materials, Cambridge university press, 1994.
[50] T. Hughes, J. Cottrell, Y. Bazilevs, Isogeometric analysis: CAD, finite elements, NURBS, exact geometry and mesh refinement, Computer Methods in Applied Mechanics and Engineering 194 (39-41) (2005) 4135 – 4195.
[51] Y. Lai, Y. J. Zhang, L. Liu, X. Wei, E. Fang, J. Lua, Integrating CAD with Abaqus: A practical isogeometric analysis software platform for industrial applications, Computers & Mathematics with Applications .
[52] Y. Lu, Construction d'abaques numériques dédiés aux études paramétriques du procédé de soudage par des méthodes de réduction de modèles espace-temps, Ph.D. thesis, Université de Lyon, 2017.
[53] H.-J. Bungartz, M. Griebel, Sparse grids, Acta numerica 13 (2004) 147–269.